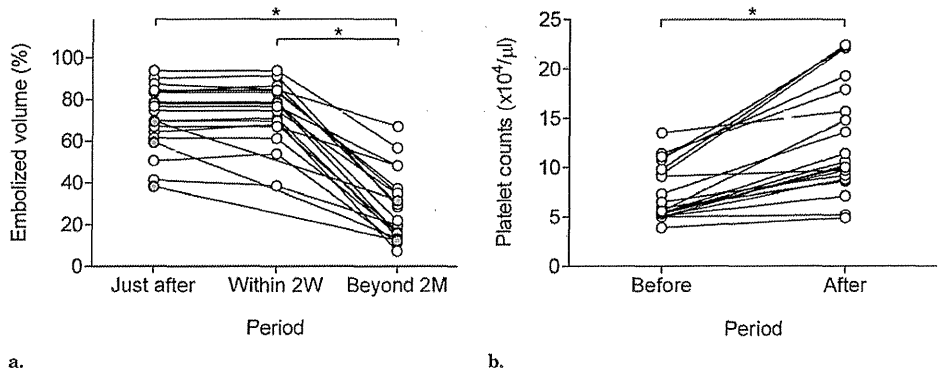

Figure 2. Time courses of spleen infarction rate and platelet count after PSE. **(a)** The median spleen embolization rate for 20 cases was 72.1% (IQR, 38.2%–93.8%) when evaluated immediately after the completion of PSE. After 2 months (*M*) or more, the ratio significantly reduced to 25.2% (IQR, 7.2–66.9%), although it did not significantly change within the first 2 weeks (*W*) after PSE (median, 76.6%, IQR, 38.4%–93.8%) in 17 cases. The gray circles indicate three cases that did not undergo CT within 2 weeks of the procedure. **(b)** The platelet counts significantly increased from 5.8 × $10^4/\mu L$ (IQR, 3.9–13.5 × 10^4/mL) before PSE to 10.4 × 10^4/mL (IQR, 4.9–22.4 × $10^4/\mu L$) at the stable post-PSE period. Asterisks indicate significant differences at $P < .0001$.

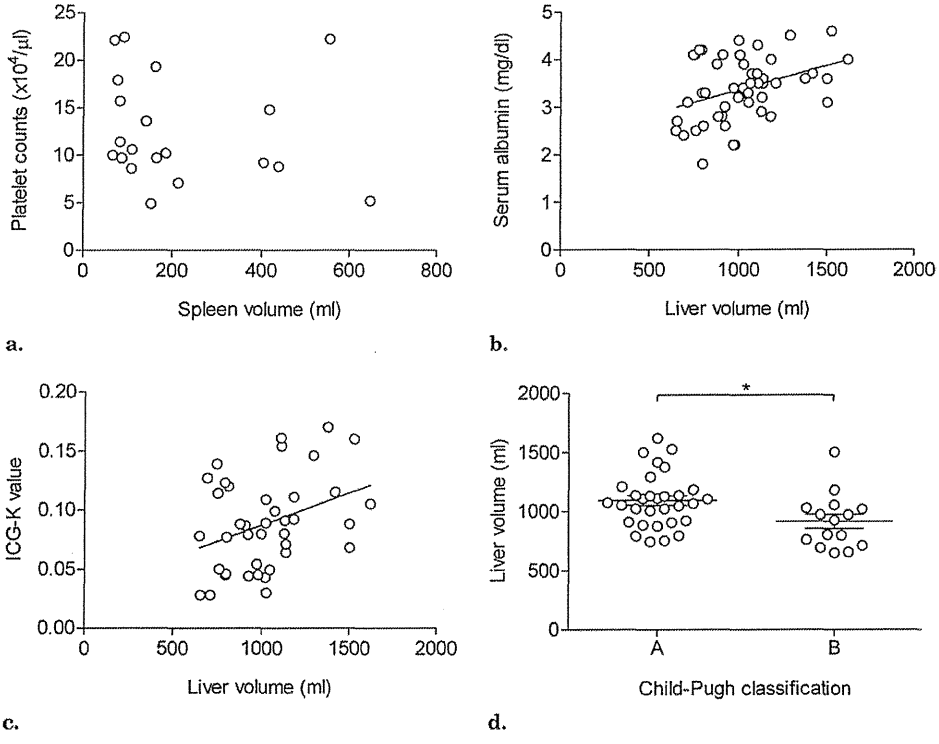

Figure 3. Relationships between Vsp and platelet count and between Vh and functional liver reserve. **(a)** The platelet count did not correlate with the Vsp after PSE in 20 cases with hypersplenism ($P = .15$, $\rho = -0.34$). In 51 patients with cirrhosis, the Vh revealed a significant positive correlation with **(b)** the serum albumin concentration ($P = .013$, $\rho = 0.35$) and with **(c)** the rate of disappearance of ICG from the circulation (*ICG-K*; $P = .042$, $\rho = 0.32$). **(d)** Vh was significantly smaller in patients with cirrhosis with a lower hepatic reserve (Child–Pugh class B disease, n = 15) than in patients with cirrhosis with a higher hepatic reserve (Child–Pugh class A disease, n = 31). The asterisk indicates a *P* value of .012.

with the serum albumin concentration ($P = .013$, $\rho = 0.35$; **Fig 3b**) or the rate of disappearance of ICG from the bloodstream ($P = .042$, $\rho = 0.32$; **Fig 3c**) in 51 consecutive cases of various types of liver cirrhosis, significant positive correlations were observed. In addition, as shown in **Figure 3d**, Vh was significantly larger in the 31 cases of Child–Pugh class A disease than in the 15 cases of Child–Pugh class B disease ($P = .012$).

Significant Correlations between Platelet Count and CT Volume Data

Multiple linear regressions were performed by using the six variables of pre-PSE platelet count, pre-PSE Vsp, pre-PSE Vh, eVsp, eVsp%, and pre-PSE Vh/Vsp ratio to predict the platelet count increase ratio (dPlt%) in a stepwise method (**Table 2**). eVsp% and pre-PSE Vh/Vsp ratio were selected

Table 2. Multivariate Analysis to Predict Platelet Count Increase Ratio

Model	Predictor	Standardized Coefficient	*P* Value of Predictor	Excluded Factor	*P* Value of Factor
1	eVsp	0.579	.001	Platelets before PSE	.295
				Vsp before PSE	.003
				Vh before PSE	.160
				eVsp%	.002
				Vh/Vsp before PSE	.698
2	eVsp	0.503	.001	Platelets before PSE	.104
				Vsp before PSE	.727
	eVsp%	0.446	.002	Vh before PSE	.064
				Vh/Vsp before PSE	.035
3	eVsp	0.267	.113	Platelets before PSE	.217
	eVsp%	0.573	.000	Vsp before PSE	.433
	Vh/Vsp before PSE	−0.367	.035	Vh before PSE	.724
4	eVsp%	0.660	.000	Platelets before PSE	.233
				Vsp before PSE	.169
	Vh/Vsp before PSE	−0.544	.000	Vh before PSE	.269
				eVsp	.113

Note.—eVsp = spleen embolization volume, eVsp% = spleen embolization ratio, PSE = partial splenic arterial embolization, Vh = hepatic volume, Vsp = splenic volume.

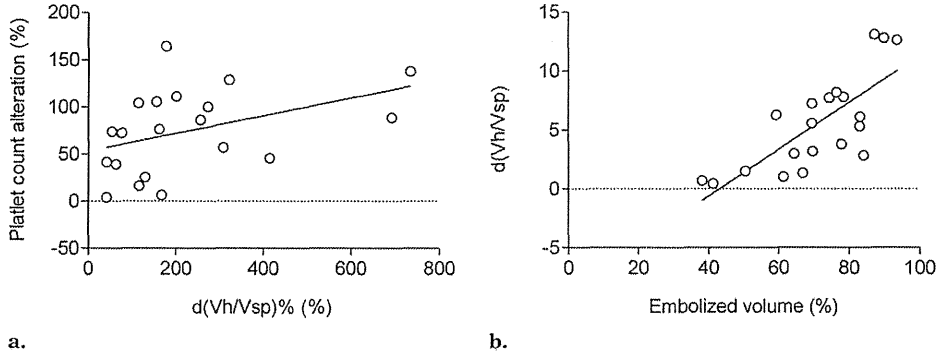

Figure 4. Correlations among variables after PSE. **(a)** An increase in the percentage of platelet counts after PSE significantly correlated with an alteration in Vh/Vsp ratio (as a percentage) after PSE ($P = .019$, $\rho = 0.52$). **(b)** The difference in Vh/Vsp ratio before and after PSE significantly correlated with eVsp (as a percentage of the total before PSE; $P = .0003$, $\rho = 0.72$).

as significant variables, with a probability of less than 0.001 for each. Consistently, dPlt% showed a significant positive correlation with d(Vh/Vsp)% ($P = .019$, $\rho = 0.52$; **Fig 4a**). The linear regression line was as follows:

$$dPlt\% = 9.37 \times d(Vh/Vsp)\% + 53.13$$

In addition, d(Vh/Vsp) and eVsp% showed a significant positive correlation ($P = .0003$, $r = 0.72$; **Fig 4b**) as follows:

$$d(Vh/Vsp) = 0.199 \times eVsp\% - 8.58$$

Prediction of Platelet Count after PSE Based on Liver and Spleen CT Volume Data

By substituting d(Vh/Vsp) with a function of eVsp%, dPlt% can be expressed by using only factors that are obtained from the PSE procedure as follows:

$$dPlt\% = (1.86 \times eVsp\% - 80.39)/\text{pre-PSE Vh/Vs-pratio} + 53.13$$

When the actual dPlt% was compared with the dPlt% estimated from the aforementioned formula, the two factors were significantly correlated ($P = .0003$, $r = 0.72$; **Fig 5a**). The correlation between the actual and estimated dPlt% was further evaluated in 14 other consecutive cases treated with PSE, revealing a strict positive correlation ($P < .0001$, $\rho = 0.92$; **Fig 5b**). By adjusting the percentage to an absolute value, the estimated platelet count after PSE was predicted by using a new formula:

Estimated platelets = pre-PSE platelets + pre-PSE platelets × [(4.393 × eVsp% − 189.32)/pre-PSE Vh/Vs-pratio + 39.93]/100

DISCUSSION

PSE was originally performed as a "medical splenectomy" in an attempt to control variceal bleeding in conditions of hypersplenism (8), and its application has since been extended to the treatment of thrombocytopenia. In HCV-positive cases,

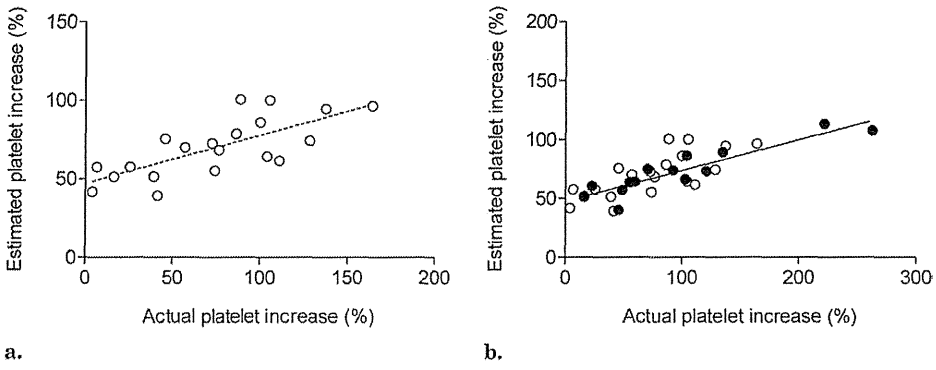

Figure 5. A significant correlation was seen between the estimated and actual platelet count increases after PSE. An increase in the percentage of platelet counts after PSE was estimated by using the formula (1.86 × eVsp% − 80.39)/pre-PSE Vh/Vsp ratio + 53.13. **(a)** The estimated platelet increase significantly correlated with the actual platelet increase in the initial cohort, from which the formula was deduced ($P = .0003$, $\rho = 0.72$). **(b)** The estimated platelet increase significantly correlated with the actual platelet increase in the subsequent independent test cohort ($P < .0001$, $\rho = 0.92$). Open circles indicate the initial formula-deducing cohort; closed circles indicate the testing cohort. The dotted and solid lines are correlation lines for the initial cohort and the testing cohort, respectively.

thrombocytopenia frequently undermines attempts to eradicate HCV by using interferon (1). Hepatocellular carcinoma predominantly develops in cirrhotic livers in individuals with low platelet counts and subsequently hinders the application of several treatment options. Although PSE is preferable to splenectomy because it is less invasive (17–19), it is still an invasive procedure and can be accompanied by severe or fatal complications (14). A poor functional liver reserve and larger infarction volume are risk factors for complications (13). As effect and risk represent trade-offs (10), it is ideal to embolize only enough volume to achieve the required gain in platelet numbers. To achieve this goal, it is necessary to be able to make a practical prediction of the platelet count after PSE; however, to our knowledge, a method for making such a prediction has not been developed until now. In the present report, we developed a formula to predict the platelet count after PSE based on CT volumetry. The strength of the prediction was confirmed in 14 test cases. For example, the formula indicates that approximately half of the spleen should be embolized to achieve a 50% gain in platelet count if the Vsp is half the Vh before PSE. A calculator for the formula is available online (http://www.med.niigata-u.ac.jp/in3/resident/PSE.html). The only required input parameters are Vh and Vsp before PSE. If the anticipated infarction rate of the spleen is used as an input, the calculator returns percent platelet gain after PSE, or vice versa. A feasible prediction would help an operator decide the necessary volume and intensity of embolization. In addition, the prediction would aid in planning sequential PSE to avoid risk by minimizing each embolization and achieving the final goal. The lack of different responses in platelet count among etiologies of liver cirrhosis suggests that the formula can be used in a wide variety of backgrounds.

Several lines of evidence suggest that thrombocytopenia develops as a multifactorial condition in individuals with cirrhosis (6). The sequestration of platelets by the spleen likely plays a key role. In terms of impaired thrombopoiesis, the circulating thrombopoietin level is solely controlled by binding to its receptor, c-mpl, on circulating platelets (20,21), instead of the thrombopoietin gene being subject to transcriptional control (22–24). McMillan et al (25) demonstrated that anti-GPIIb/IIIa autoantibodies derived from patients with idiopathic thrombocytopenic purpura suppressed the production and maturation of megakaryocytes in vitro (25). Patients with cirrhosis frequently produce anti-GPIIb/IIIa autoantibodies (26), suggesting that a similar pathway is active in cirrhosis. In addition, platelet turnover is accelerated in patients with cirrhosis (27). Although the mechanism is still under debate, the fact that cirrhotic thrombocytopenia increases in incidence and intensity as the severity of various liver diseases increases (1,2,15) indicates that a primary pathogenic process is shared between cirrhosis and thrombocytopenia. Based on this hypothesis, we sought to incorporate a surrogate functional liver reserve factor into our formula.

It has been reported that Vh is correlated with the values for quantitative tests for hepatic reserve, such as technetium-99m galactosyl human serum albumin scintigraphy (28) or the formation rate of lidocaine metabolite (29). An improvement in protein synthesis has also been reported to correlate with an increasing Vh after splenectomy (30). In addition, in our cohort, the Vh was significantly larger in cases of Child–Pugh class A disease than in cases of Child–Pugh class B disease, and was significantly correlated with serum albumin concentration and with the disappearance rate of ICG (31). Multivariate analysis supports the notion that the platelet count is defined by the balance between the destruction and the production of platelets. eVsp% and pre-PSE Vh/Vsp ratio were selected as factors from which to predict dPlt%; therefore, we explored the correlation between dPlt% and d(Vh/Vsp)%. Although post-PSE Vh/Vsp ratio cannot be directly calculated during the procedure, a correlation analysis revealed that d(Vh/Vsp) was significantly associated with eVsp%. We recommend defining eVsp% from CT images obtained

within 2 weeks of PSE because eVsp% was stable for these 2 weeks, whereas the Vsp substantially changed after this time, leading to a gradual decrease in eVsp% over time.

One limitation of the present study is the relatively small number of cases, which may have resulted in an inadequate assessment of biologic variability. Given that PSE was repeated in only three cases, the prediction after the second round of sequential PSE may be inaccurate. Watanabe et al (32) reported that thrombocytosis induced a reduction in liver fibrosis in mice. Although Vh did not significantly change after PSE in our cohort, whether Vh changes after PSE is controversial. Murata et al (30) reported that Vh increased after PSE, whereas Vh did not significantly change according to a report by Tomikawa et al (33). If the relationship between the functional liver reserve and thrombopoiesis is altered after PSE, this change would affect the performance of our formula. In addition, although the CT scan and platelet counts were performed on the same day in most cases, there was an interval of as long as 26 days in nine cases, and Vh/Vsp may have changed during this interval. To confirm the accuracy of the formula, a prospective study in a larger cohort is necessary.

In conclusion, we have developed a formula to predict the platelet count after PSE. The formula is based on liver and spleen CT volumetry, and the embolization rate is converted into a feasible prediction of the platelet count. Use of the formula will contribute to physical fitness and quality of life in patients with hypersplenism by enhancing the safety and efficacy of PSE. When the efficacy of our formula has been confirmed in a prospective study with a larger cohort, it will be an important way to calculate eVsp without a CT scan.

REFERENCES

1. Tejima K, Masuzaki R, Ikeda H, et al. Thrombocytopenia is more severe in patients with advanced chronic hepatitis C than B with the same grade of liver stiffness and splenomegaly. J Gastroenterol 2010; 45:876–884.
2. Olariu M, Olariu C, Olteanu D. Thrombocytopenia in chronic hepatitis C. J Gastrointest Liver Dis 2010; 19:381–385.
3. Ando E, Yamashita F, Tanaka M, Tanikawa K. A novel chemotherapy for advanced hepatocellular carcinoma with tumor thrombosis of the main trunk of the portal vein. Cancer 1997; 79:1890–1896.
4. Ota H, Nagano H, Sakon M, et al. Treatment of hepatocellular carcinoma with major portal vein thrombosis by combined therapy with subcutaneous interferon-alpha and intra-arterial 5-fluorouracil; role of type 1 interferon receptor expression. Br J Cancer 2005; 93:557–564.
5. Takayasu K, Arii S, Ikai I et al. Prospective cohort study of transarterial chemoembolization for unresectable hepatocellular carcinoma in 8510 patients. Gastroenterology 2006; 131:461–469.
6. Poordad F. Review article: thrombocytopenia in chronic liver disease. Aliment Pharmacol Ther 2007; 1:5–11.
7. Tajiri T, Onda M, Yoshida H, Mamada Y, Taniai N, Kumazaki T. Long-term hematological and biochemical effects of partial splenic embolization in hepatic cirrhosis. Hepatogastroenterology 2002; 49:1445–1448.
8. Maddison FE. Embolic therapy of hypersplenism. Invest Radiol 1973; 8:280–281.
9. Noguchi H, Hirai K, Aoki Y, Sakata K, Tanikawa K. Changes in platelet kinetics after a partial splenic arterial embolization in cirrhotic patients with hypersplenism. Hepatology 1995; 22:1682–1688.
10. Hayashi H, Beppu T, Masuda T, et al. Predictive factors for platelet increase after partial splenic embolization in liver cirrhosis patients. J Gastroenterol Hepatol 2007; 22:1638–1642.
11. Wang HY, Shih SC, Lin SC, et al. Partial splenic embolization: 12-month hematological effects and complications. Hepatogastroenterology 2008; 55:1838–1842.
12. Han MJ, Zhao HG, Ren K, Zhao DC, Xu K, Zhang XT. Partial splenic embolization for hypersplenism concomitant with or after arterial embolization of hepatocellular carcinoma in 30 patients. Cardiovasc Intervent Radiol 1997; 20:125–127.
13. Hayashi H, Beppu T, Okabe K, Masuda T, Okabe H, Baba H. Risk factors for complications after partial splenic embolization for liver cirrhosis. Br J Surg 2008; 95:744–750.
14. Castaneda-Zuniga WR, Hammerschmidt DE, Sanchez R, Amplatz K. Nonsurgical splenectomy. AJR Am J Roentgenol 1977; 129:805–811.
15. Giannini EG, Botta F, Borro P, et al. Application of the platelet count/spleen diameter ratio to rule out the presence of oesophageal varices in patients with cirrhosis: a validation study based on follow-up. Dig Liver Dis 2005; 37:779–785.
16. Sacks D, McClenny TE, Cardella JF, Lewis CA. Society of Interventional Radiology clinical practice guidelines. J Vasc Interv Radiol. 2003; 14(suppl):S199–S202.
17. Foruny JR, Blazquez J, Moreno A, et al. Safe use of pegylated interferon/ribavirin in hepatitis C virus cirrhotic patients with hypersplenism after partial splenic embolization. Eur J Gastroenterol Hepatol 2005; 17:1157–1164.
18. Kauffman CR, Mahvash A, Kopetz S, Wolff RA, Ensor J, Wallace MJ. Partial splenic embolization for cancer patients with thrombocytopenia requiring systemic chemotherapy. Cancer 2008; 112:2283–2288.
19. Hidaka H, Kokubu S, Nakazawa T, et al. Therapeutic benefits of partial splenic embolization for thrombocytopenia in hepatocellular carcinoma patients treated with radiofrequency ablation. Hepatol Res 2009; 39: 772–778.
20. Wolber EM, Ganschow R, Burdelski M, Jelkmann W. Hepatic thrombopoietin mRNA levels in acute and chronic liver failure of childhood. Hepatology 1999; 29:1739–1742.
21. Shimodaira S, Ishida F, Ichikawa N, et al. Serum thrombopoietin (c-Mpl ligand) levels in patients with liver cirrhosis. Thromb Haemost 1996; 76:545–548.
22. Kawasaki T, Takeshita A, Souda K, et al. Serum thrombopoietin levels in patients with chronic hepatitis and liver cirrhosis. Am J Gastroenterol 1999; 94:1918–1922.
23. Fielder PJ, Gurney AL, Stefanich E, et al. Regulation of thrombopoietin levels by c-mpl-mediated binding to platelets. Blood 1996; 87:2154–2161.
24. Li J, Xia Y, Kuter DJ. Interaction of thrombopoietin with the platelet c-mpl receptor in plasma: binding, internalization, stability and pharmacokinetics. Br J Haematol 1999; 106:345–356.
25. McMillan R, Wang L, Tomer A, Nichol J, Pistillo J. Suppression of in vitro megakaryocyte production by antiplatelet autoantibodies from adult patients with chronic ITP. Blood 2004; 103:1364–1369.
26. Kajihara M, Kato S, Okazaki Y, et al. A role of autoantibody-mediated platelet destruction in thrombocytopenia in patients with cirrhosis. Hepatology 2003; 37:1267–1276.
27. Kajihara M, Okazaki Y, Kato S, et al. Evaluation of platelet kinetics in patients with liver cirrhosis: similarity to idiopathic thrombocytopenic purpura. J Gastroenterol Hepatol 2007; 22:112–118.
28. Nanashima A, Yamaguchi H, Shibasaki S, et al. Relationship between CT volumetry and functional liver volume using technetium-99m galactosyl serum albumin scintigraphy in patients undergoing preoperative portal vein embolization before major hepatectomy: a preliminary study. Dig Dis Sci 2006; 51:1190–1195.
29. Lee WC, Chen MF. Assessment of hepatic reserve for indication of hepatic resection: how I do it. J Hepatobiliary Pancreat Surg 2005; 12:23–26.
30. Murata K, Ito K, Yoneda K, Shiraki K, Sakurai H, Ito M. Splenectomy improves liver function in patients with liver cirrhosis. Hepatogastroenterology 2008; 55:1407–1411.
31. Zipprich A, Kuss O, Rogowski S, et al. Incorporating indocyanine green clearance into the Model for End Stage Liver Disease (MELD-ICG) improves prognostic accuracy in intermediate to advanced cirrhosis. Gut 2010; 59:963–968.
32. Watanabe M, Murata S, Hashimoto I, et al. Platelets contribute to the reduction of liver fibrosis in mice. J Gastroenterol Hepatol 2009; 24:78–89.
33. Tomikawa M, Hashizume M, Akahoshi T, et al. Effects of splenectomy on liver volume and prognosis of cirrhosis in patients with esophageal varices. J Gastroenterol Hepatol 2002; 17:77–80.

Leukemia Research 36 (2012) 1035–1040

Contents lists available at SciVerse ScienceDirect

Leukemia Research

journal homepage: www.elsevier.com/locate/leukres

Impairment in differentiation and cell cycle of thymocytes by loss of a *Bcl11b* tumor suppressor allele that contributes to leukemogenesis

Rieka Go[a], Kazuyoshi Takizawa[a,b], Satoshi Hirose[a], Yoshinori Katsuragi[a], Yutaka Aoyagi[b], Yukio Mishima[a], Ryo Kominami[a,*]

[a] Department of Molecular Genetics, Graduate School of Medical and Dental Sciences, Niigata University, Niigata, Japan
[b] 3rd Department of Internal Medicine, Graduate School of Medical and Dental Sciences, Niigata University, Niigata, Japan

ARTICLE INFO

Article history:
Received 27 December 2011
Received in revised form 28 April 2012
Accepted 28 April 2012
Available online 27 May 2012

Keywords:
T-ALL
BCL11B
Type B abnormalities
Haploinsufficiency
Cell cycle of thymocytes

ABSTRACT

Genetic changes in T-ALL are classified into type A abnormalities leading to arrest at a specific stage of T-cell differentiation and type B abnormalities that target cellular processes including cell cycle regulation. Mutations and deletion of a *BCL11B* haploinsuffiecient tumor suppressor allele have been found in 10–16% of T-ALL subgroups. Analysis of *Bcl11b*$^{KO/+}$ mice revealed impaired T-cell differentiation at two different stages and attenuation of γ-ray induced cell-cycle arrest at S/G2/M phase in immature CD8 single positive cells. Hence, those phenotypes provided by loss of a *Bcl11b* allele favor that *Bcl11b* mutation belongs to type B abnormalities.

1. Introduction

T-cell acute lymphoblastic leukemia (T-ALL) is a common pediatric leukemia and an aggressive malignancy of thymocytes that accounts for about 15% of ALL cases [1,2]. Leukemic transformation of immature thymocytes is caused by a multistep pathogenesis involving numerous genetic abnormalities that drive normal T-cells into uncontrolled cell growth and clonal expansion. Despite the diversity in genetic alterations, the biological processes that are targeted seem conserved throughout all T-ALL cases and affect T-cell differentiation, T-cell receptor signaling that affects cell survival, and cell cycle. The current knowledge of oncogenic and tumor suppressive mutations in T-ALL suggests a classification of these genetic defects into type A and type B abnormalities [3]. Type A abnormalities such as *TAL/LMO* alterations are a class that delineates distinct molecular-cytogenetic T-ALL subgroups and are thought to cause arrest at a specific stage of normal T-cell differentiation. The other class is type B abnormalities including *CDKN2A/2B* and *NOTCH1* mutations that are shared by several different T-ALL subgroups, and they target cellular processes including cell cycle regulation and synergize with the type A mutations during T-cell pathogenesis.

Bcl11b (B-cell CLL/lymphoma 11b) belongs to Kruppel-like C_2H_2 type zinc finger transcription proteins, the largest family of transcription factors in eukaryotes [4–7]. Although *Bcl11b* knockout (KO) mice die shortly after birth, loss of Bcl11b function is known to lead to arrest of thymocyte differentiation at different stages, indicating many roles in T-cell development [8–13]. The *Bcl11b* gene was first identified as a tumor suppressor gene by analysis of γ-ray induced mouse thymic lymphomas [4,14], a model of T-ALL [15], and genetic changes were found in more than a half of the lymphomas [4,16,17]. Recently, mutations and deletions of the human orthologue *BCL11B* have been found in 10–16% of T-ALL [18–20], and of interest, these mutations are detected irrespective of T-ALL subgroups. Accordingly, *Bcl11b* mutation may be classified into a type B abnormality, though consequences of the mutation were not investigated.

One characteristic of *Bcl11b* is haploinsufficient in its tumor suppressive capability, one wild-type allele being insufficient for tumor suppression. This is based on that most of the thymic lymphomas developed in *Bcl11b*$^{KO/+}$ mice retained the wild-type allele although thymic lymphomas developed in wild-type mice showed loss of one *Bcl11b* allele at a high frequency [16,17]. The retention of the wild-type allele was observed in spontaneously developed thymic lymphomas in *Bcl11b*$^{KO/+}$*p53*$^{KO/+}$ mice [16], and importantly, also in T-ALLs having mutations on the *BCL11B* gene [19,20]. These indicate that only loss of one *Bcl11b* allele can affect lymphomagenesis

* Corresponding author at: Department of Molecular Genetics, Graduate School of Medical and Dental Sciences, Niigata University, Asahimachi 1-757, Niigata 951-8510, Japan. Tel.: +81 25 227 2077; fax: +81 25 227 0757.
E-mail address: rykomina@med.niigata-u.ac.jp (R. Kominami).

0145-2126/$ – see front matter © 2012 Elsevier Ltd. All rights reserved.
http://dx.doi.org/10.1016/j.leukres.2012.04.028

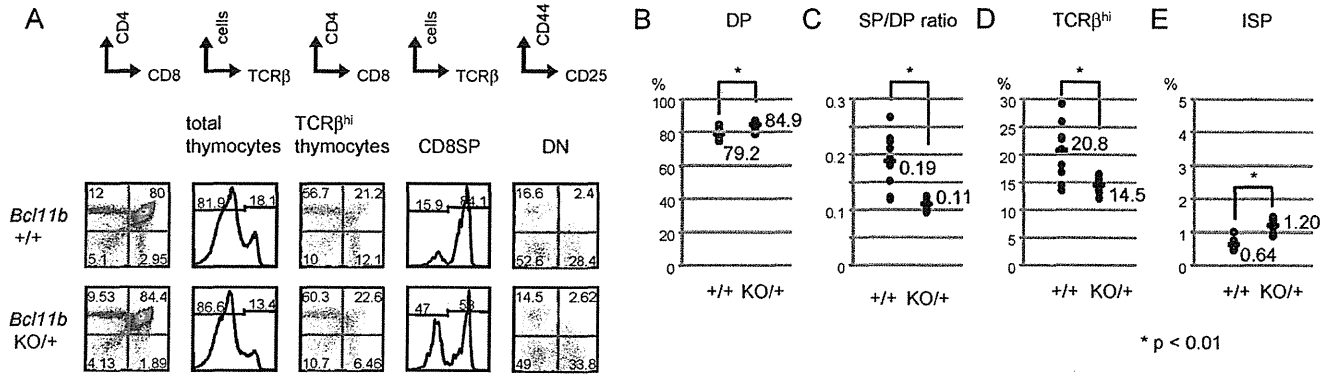

Fig. 1. Effect of *Bcl11b*$^{KO/+}$ genotype on differentiation of thymocytes. (A) Flow cytometric analysis of thymocytes from *Bcl11b*$^{+/+}$ and *Bcl11b*$^{KO/+}$ mice using CD4, CD8, TCRβ, CD25 and CD44 markers. The markers used are indicated above in each panel. As for TCRβ expression on thymocytes, total thymocytes (left) and cells in the CD4$^-$CD8$^+$ quadrant (right) were analyzed. (B, D, E) The percentage of cells and the absolute number in thymocyte subsets: B, DP cells; D, TCRβ^{high} thymocytes; E, ISP cells. (C) The ratio of SP cells/DP cells. The absolute number in average is shown below each number of the percentage. Comparison was performed between *Bcl11b*$^{+/+}$ (n=9) and *Bcl11b*$^{KO/+}$ (n=11) mice. *P* value for difference in the percentage between *Bcl11b*$^{+/+}$ and *Bcl11b*$^{KO/+}$ mice is less than 5% in each of B, C, D and E.

in mice and humans. Haploinsufficient capability of *Bcl11b* is also reported in tissue development [21,22]. Despite the importance of *Bcl11b* heterozygosity in lymphomagenesis, its effect on T-cell development was not studied in detail. Hence, we have examined differentiation, apoptosis, and cell cycle of thymocytes at different developmental stages in *Bcl11b*$^{KO/+}$ mice. In this paper we show that loss of a *Bcl11b* allele leads to differentiation arrest at certain immature stages and deregulation of the response to γ-radiation in cell cycle, a phenotype that may be explained by the type B alteration.

2. Materials and methods

2.1. Mice

Bcl11b$^{KO/+}$ mice were generated as described [5]. *Bcl11b*$^{+/+}$ and *Bcl11b*$^{KO/+}$ mice of the BALB/c background were subjected to γ-irradiation of 1 Gy or 3 Gy at 8 weeks of age as described [23]. Thymus or left and right thymic lobes were isolated at indicated times after irradiation and subjected to analysis. Mice used in this study were maintained under specific pathogen-free conditions in the animal colony of Niigata University. All animal experiments comply with the guidelines by the animal ethics committee for animal experimentation of the university.

2.2. Flow cytometry

Flow cytometric analysis was performed as previously described [5]. In brief, single cell suspensions of thymocytes were prepared from thymus and, $1–2 \times 10^6$ cells were incubated with antibodies in phosphate-buffered saline containing 2% fetal calf serum and 0.2% NaN_3 for 15 min at 4 °C. The monoclonal antibodies (mAbs) used were anti-CD4-APC or -PerCP-Cy5.5 (RM4-5 BioLegend), anti-CD8-APC or -PE (53-6.7 eBioscience), anti-CD25-FITC (PC61 BioLegend), anti-CD44-PE (IM7 Biolegend), and anti-TCRβ-FITC or -APC (H57-597 BioLegend). To prevent non-specific binding of mAbs, we added CD16/32 (93 eBioscience) before staining with labeled mAbs. Dead cells and debris were excluded from the analysis by appropriate gating of FSC and SSC. Cells were analyzed by a FACScan or a FACSCalibur (Becton-Dickinson) flow cytometer, and data were analyzed using the Flow-Jo software (Tree-Star, Inc.).

Apoptosis was measured by Annexin V assay following the manufacturer's instructions (BD Bioscience). Briefly, thymocytes were washed in cold PBS and resuspended in binding buffer (HEPES buffer supplemented with 2.5 mM $CaCl_2$). These were incubated with FITC-labeled Annexin V (BD Bioscience) for 15 min at room temperature. Flow cytometry was performed on thymocytes gated on the basis of their forward and side light scatter with any cell debris excluded from analysis. Apoptotic cells were defined as FITC$^+$ cells.

For BrdU incorporation experiments, we injected mice intra-peritoneally with 100 μl of BrdU solution (10 mg/ml). In indicated cases, irradiation was performed at 1 h after BrdU injection. Thymuses were isolated 1 h or 5 h after BrdU administration and thymocytes were fixed with cytofix/Cytoperm (BD Bioscience) and analyzed with the use of the BD Bioscience BrdU Flow Kit according to Manufacturer's instruction. In brief, cells were suspended at a concentration of $1–2 \times 10^6$ cells/ml, fixed, permeabilized and incubated with DNaseI (300 μg/ml) for 60 min at 37 °C. After washing, cells were incubated with FITC conjugated anti-BrdU antibodies for 20 min at room temperature. Cells were resuspended in staining buffer and analyzed by FACSCalibur flow cytometer.

Statistical analysis was done using *t*-test.

3. Results

3.1. Differentiation of thymocytes

Development of αβ T cells in the thymus proceeds through three major stages defined according to their expression pattern of CD4 and CD8 molecules on cell surface, i.e. in order of maturity, CD4$^-$CD8$^-$ double negative (DN), CD4$^+$CD8$^+$ double positive (DP), and CD4$^+$CD8$^-$ or CD4$^-$CD8$^+$ single positive cells (CD4SP or CD8SP cells, respectively) [7,24]. DP thymocytes undergo rearrangement at the TCRα locus and hence a small fraction (TCRβ^{high}-DP cells) expresses the αβ T-cell receptor (TCRαβ) complex on cell surface before progressing to TCRβ^{high}-SP stage. Immature CD8$^+$ single positive (ISP) cells exist between DN and DP stages, and they express CD8 but lack αβ TCR. DN thymocytes can be further divided into four subpopulations based on the surface expression of CD44 and CD25, with the developmental progression being CD44$^+$CD25$^-$ (DN1) to CD44$^+$CD25$^+$ (DN2) to CD44$^-$CD25$^+$ (DN3) and then to CD44$^-$CD25$^-$ (DN4) cells.

Fig. 1A shows flow cytometric analysis of thymocytes using differentiation markers that were obtained from *Bcl11b*$^{+/+}$ wild-type and *Bcl11b*$^{KO/+}$ heterozygous mice. Fig. 1B, D and E show the percentage of DP, TCRβ^{high} and ISP cells, respectively, and Supplementary Fig. 1A–D shows the absolute cell number of the thymocyte subsets. Analysis with CD4 and CD8 markers showed a higher percentage of DP cells (Fig. 1B) and a lower ratio of SP cells/DP cells (Fig. 1C) in *Bcl11b*$^{KO/+}$ thymus than in *Bcl11b*$^{+/+}$ thymus. The absolute number of DP cells was increased in *Bcl11b*$^{KO/+}$ thymus (Supplementary Fig. 1B). These results suggest developmental arrest of a certain fraction of thymocytes at DP stage in *Bcl11b*$^{KO/+}$ mice. Expression of TCRβ marker in total thymocytes showed a significantly decreased percentage of TCRβ^{high} cells in *Bcl11b*$^{KO/+}$ mice (Fig. 1D). This suggests arrest at TCRβ^{low} DP stage possibly before rearrangement at the TCRα locus.

Cells in the CD8$^+$ fraction consist of mature CD8SP cells highly expressing TCRβ and immature ISP cells with much lower expression. The percentage and the absolute number of ISP cells were higher in *Bcl11b*$^{KO/+}$ thymus than *Bcl11b*$^{+/+}$ thymus (Fig. 1E and Supplementary Fig. 1A), suggesting arrest also at the ISP stage. The CD8$^+$ fraction may include γδ T cells [10]. However, their

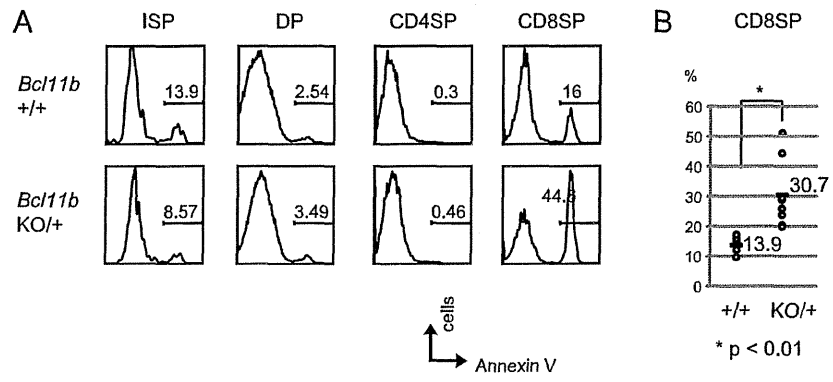

Fig. 2. Comparison of apoptosis in thymocytes from *Bcl11b*$^{+/+}$ and *Bcl11b*$^{KO/+}$ mice. (A) Flow cytometric analysis of Annexin V-positive cells in the thymocyte subsets indicated above. The vertical axis shows cell numbers and the horizontal axis shows Annexin V-expression levels. (B) The percentage of Annexin V-positive cells in thymocyte subsets. Comparison was performed between *Bcl11b*$^{+/+}$ ($n=6$) and *Bcl11b*$^{KO/+}$ ($n=8$) mice. *P* values for difference in ISP and CD8SP subsets are less than 1%.

percentage was very low in *Bcl11b*$^{+/+}$ and *Bcl11b*$^{KO/+}$ CD8$^+$ fractions and no marked difference was observed between them (Supplementary Fig. 2), indicating that the higher percentage of ISP cells is due to an accumulation of precursors to DP cells. On the other hand, analysis of DN cell subtypes using CD44 and CD25 markers did not show significant differences in the percentage or the cell number between *Bcl11b*$^{+/+}$ and *Bcl11b*$^{KO/+}$ mice (Supplementary Fig. 3). This suggests no impairment during development of immature DN thymocytes. Together, these results suggest developmental arrest at the two different ISP and DP stages in *Bcl11b*$^{KO/+}$ heterozygous mice.

3.2. Apoptosis and proliferation of thymocytes

T-cell development is tightly related to apoptosis. Accordingly, we examined the percentage of Annexin V-positive cells, an indicator of apoptosis (Fig. 2A). Annexin V$^+$ cells were observed in CD8SP cells at a significant level but very low in ISP, DP and CD4SP cells. Comparison between *Bcl11b*$^{+/+}$ and *Bcl11b*$^{KO/+}$ CD8SP thymocytes revealed a 3-fold increase in *Bcl11b*$^{KO/+}$ mice (Fig. 2B). This suggests that loss of a *Bcl11b* allele provides increased susceptibility to apoptosis in CD8SP cells.

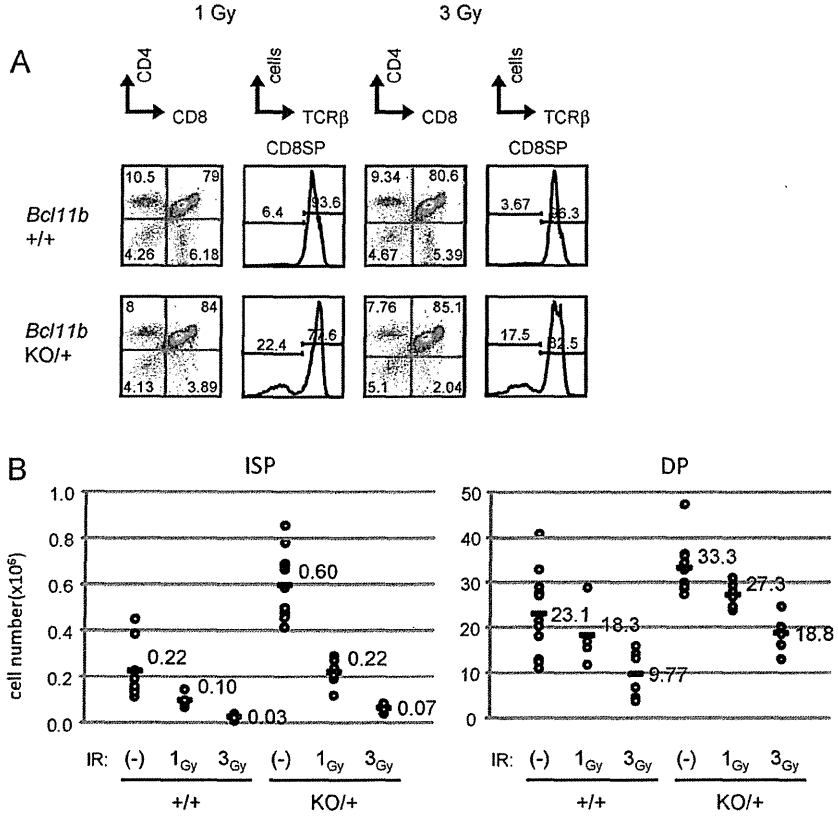

Fig. 3. Effect of γ-irradiation on the cell number in thymocytes. (A) Flow cytometric analysis of CD4, CD8 and TCRβ expression on thymocytes from 1 Gy and 3 Gy irradiated *Bcl11b*$^{+/+}$ and *Bcl11b*$^{KO/+}$ mice. Analysis was performed 4 h after irradiation. (B) The cell number of ISP and DP cells in thymic lobe after irradiation or without irradiation. The sample number is 4 in 1 Gy *Bcl11b*$^{+/+}$ mice and 6 in 1 Gy *Bcl11b*$^{KO/+}$ mice, and 6 in 3 Gy irradiated mice.

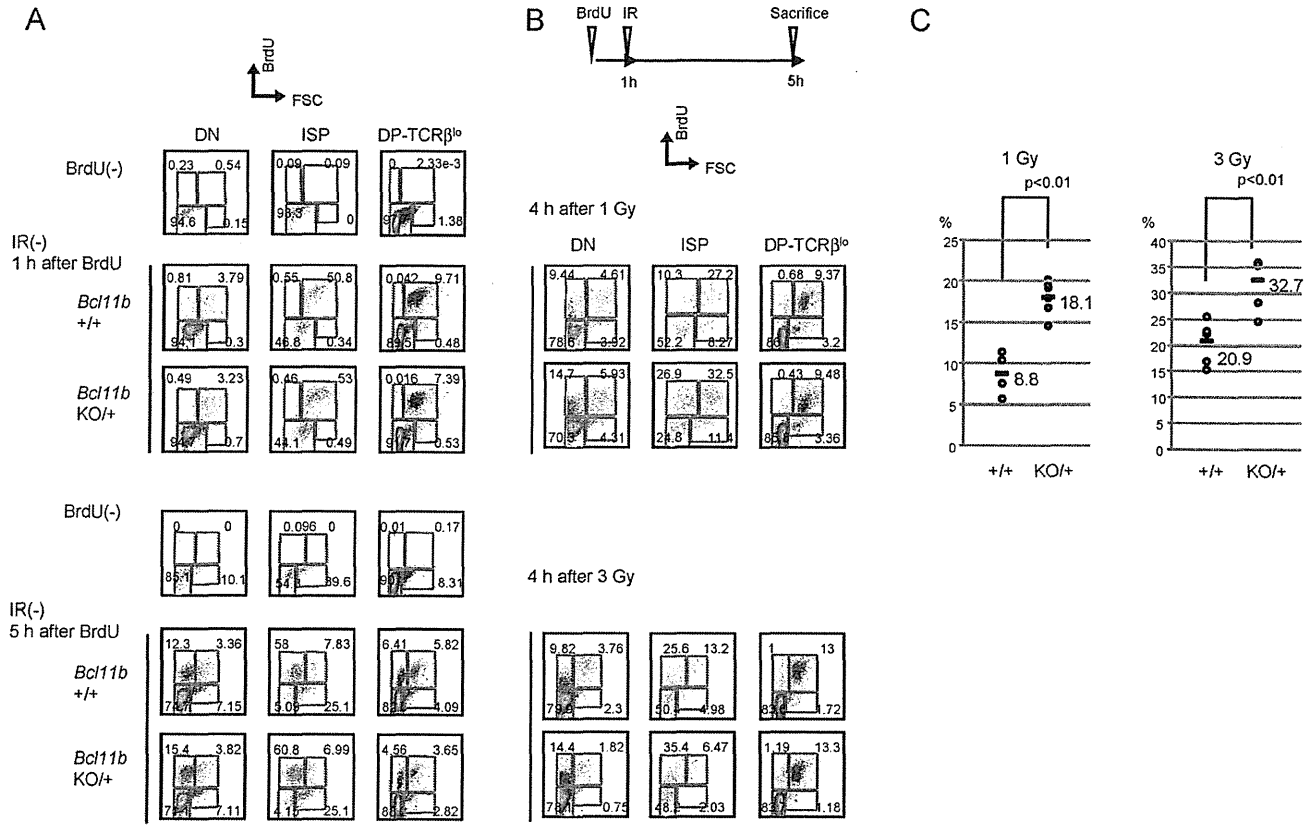

Fig. 4. Effect of γ-irradiation on cell cycle in thymocytes of *Bcl11b*$^{+/+}$ and *Bcl11b*$^{KO/+}$ mice. (A) Flow cytometric analysis of BrdU incorporation levels (vertical axis) and FSC values (horizontal axis) in thymocyte subsets in unirradiated mice. BrdU^{+}FSC^{Large} fraction represents cells in S or G2/M phases of cell cycle whereas BrdU^{+}FSC^{Small} fraction represents G1 cells that have passed S phase. (B) Flow cytometric analysis of BrdU incorporation levels and FSC values in thymocyte subsets in 1 Gy and 3 Gy irradiated mice. (C) The percentages of BrdU^{+}FSC^{S} cells in the ISP thymocyte subset in *Bcl11b*$^{+/+}$ and *Bcl11b*$^{KO/+}$ mice after 1 Gy and 3 Gy irradiation. *P* values for difference between *Bcl11b*$^{+/+}$ and *Bcl11b*$^{KO/+}$ mice after 1 Gy and 3 Gy irradiation are less than 0.5%. The sample number is 4 in 1 Gy *Bcl11b*$^{+/+}$ mice and 6 in 1 Gy *Bcl11b*$^{KO/+}$ mice, and 6 in 3 Gy irradiated mice.

Deregulation of cell cycle is a hallmark of leukemic transformation. We examined BrdU incorporation of thymocytes, an indicator of cell cycle progression, in mice 1 h after BrdU administration (Supplementary Fig. 4). About 40% of ISP cells and 8% of DP cells showed BrdU incorporation whereas very low percentages of CD4SP and CD8SP cells showed BrdU incorporation, consistent with a previous report [25]. Comparison between *Bcl11b*$^{+/+}$ and *Bcl11b*$^{KO/+}$ mice did not show significant differences in ISP and DP cells.

3.3. Effect of γ-irradiation on cellularity of thymocytes

Bcl11b$^{KO/+}$ mice developed thymic lymphomas when γ-irradiated, but not spontaneously [17]. Accordingly, of importance may be the effect of *Bcl11b*$^{KO/+}$ heterozygosity on radiation-induced cell damages. Thus, we examined cell number of thymocytes from mice 4 h after 1 Gy or 3 Gy of γ-irradiation. Fig. 3A shows expression of CD4/CD8 and TCRβ in thymocytes. Fig. 3B summarizes the cell number of ISP and DP cells in *Bcl11b*$^{+/+}$ and *Bcl11b*$^{KO/+}$ mice. One Gy irradiation led to a two-fold decrease in ISP cells and a minimal decrease in DP cells. The decreases did not differ between *Bcl11b*$^{+/+}$ and *Bcl11b*$^{KO/+}$ mice. On the other hand, 3 Gy irradiation reduced the cell number to approximately one tenth in ISP cells and to about one half in DP cells probably by inducing apoptosis differently. Comparison between *Bcl11b*$^{+/+}$ and *Bcl11b*$^{KO/+}$ mice also did not show marked difference in the decreases.

3.4. Effect of γ-irradiation on cell cycle

We next examined radiation effect on cell cycle of thymocytes. To monitor cell cycle, we administrated BrdU at 1 h before γ-irradiation. Accordingly, analysis of thymocytes was performed in mice 5 h after BrdU administration and 4 h after irradiation, and for comparison in mice 1 h and 5 h after BrdU administration without irradiation. Fig. 4A show the percentage of cells in four different areas in DN, ISP and TCRβ^{low}-DP cells in unirradiated mice. Control panels without BrdU administration are included. The four areas were determined by BrdU incorporation (vertical axis) and FSC value (horizontal axis), an indicative of cell size. BrdU^{+} FSC-large (FSC^{L}) represents cells in S or G2/M phases of cell cycle whereas BrdU^{+} FSC-small (FSC^{S}) represents G1 cells that have passed S phase after BrdU administration. BrdU^{-}FSC^{L} and BrdU^{-}FSC^{S} cells are thymocytes present in S/G2/M and G1 phase, respectively, that have not passed S phase for 5 h after BrdU administration.

In unirradiated mice 1 h after BrdU administration, the percentage of BrdU^{+}FSC^{S} cells was much less than that of BrdU^{+}FSC^{L} cells in DN, ISP, and TCRβ^{low}-DP cells irrespective of *Bcl11b*$^{+/+}$ and *Bcl11b*$^{KO/+}$ genotypes, indicating that BrdU-incorporated S-phase cells did not yet progress into G1 phase. However, in mice 5 h after, both BrdU^{+}FSC^{L} cells and BrdU^{+}FSC^{S} cells were observed at significant levels in DN, ISP, and TCRβ^{low}-DP cells. The percentage of BrdU^{+}FSC^{S} cells was more than that of BrdU^{+}FSC^{L} cells in each subset. No differences were observed between *Bcl11b*$^{+/+}$ and *Bcl11b*$^{KO/+}$

mice. These results indicated that certain fractions of thymocytes in S phase progressed to G1 phase for 4 h in those thymocyte subsets.

γ-Irradiation affected the cell cycle progression and the consequence was different depending on subsets. Fig. 4B shows the percentage of cells in four different areas in DN, ISP and TCRβ^{low}-DP cells in mice 5 h after BrdU administration and 4 h after 1 Gy or 3 Gy irradiation. TCRβ^{low}-DP cells in both irradiated mice little contained BrdU^{+}FSC^{S} cells irrespective of *Bcl11b*$^{+/+}$ or *Bcl11b*$^{KO/+}$ genotypes, indicating radiation-induced arrest at S or G2/M phase. In contrast, ISP cells comprised BrdU^{+}FSC^{S} cells at significant percentages even after irradiation, indicating the progression from S to G1 phase. One Gy irradiated mice contained more BrdU^{+}FSC^{L} cells than BrdU^{+}FSC^{S} cells whereas 3 Gy irradiated mice exhibited less BrdU^{+}FSC^{L} cells than BrdU^{+}FSC^{S} cells. Comparison between *Bcl11b*$^{+/+}$ and *Bcl11b*$^{KO/+}$ mice revealed a significant increase in the percentage of BrdU^{+}FSC^{S} cells in *Bcl11b*$^{KO/+}$ ISP cells in both 1 Gy and 3 Gy irradiated mice (Fig. 4C). Differences in radiation effect between *Bcl11b*$^{+/+}$ and *Bcl11b*$^{KO/+}$ mice were also observed in DN cells, though the DN cell fraction comprised a mixture of immature thymocytes consisting of different subsets. Together, those findings indicated that BrdU^{+}FSC^{L} ISP cells, but not BrdU^{+}FSC^{L} DP cells, progressed to BrdU^{+}FSC^{S} cells more in *Bcl11b*$^{KO/+}$ mice than *Bcl11b*$^{+/+}$ mice. This suggests that *Bcl11b*$^{KO/+}$ heterozygosity attenuates radiation-induced cell-cycle arrest at S or G2/M phase in ISP cells.

4. Discussion

This study has investigated changes in differentiation, cell survival and cell cycle during T-cell development in mice of the *Bcl11b*$^{KO/+}$ heterozygous genotype, which provides susceptibility to thymic lymphomas [4,23], a mouse model of T-ALL [15,26]. In *Bcl11b*$^{KO/+}$ mice, increases were observed in the percentage and cell number of ISP and DP cells, indicating differentiation arrest at ISP and DP stages. No impairment was observed in immature thymocytes at DN stages. Previous studies using *Bcl11b*$^{KO/KO}$ mice revealed the requirement of Bcl11b function for thymocyte differentiation at DN2 and DN3 stages [5,11–13]. These data indicate difference in the effect on differentiation between loss of one *Bcl11b* allele and loss of both alleles. The difference may be important in light of the contribution of loss of one *Bcl11b* allele alone to lymphomagenesis.

Difference in cell survival was observed between *Bcl11b*$^{KO/+}$ and *Bcl11b*$^{+/+}$ mice. The percentage of apoptotic cells in CD8SP cells was increased in *Bcl11b*$^{KO/+}$ mice. The increased apoptosis may be related to impairment in TCR (T-cell receptor) signaling that provides signaling for cell survival. This is because CD4-Cre; *Bcl11b*$^{flox/flox}$ mice lacking Bcl11b activity after DP stage fail to express a TCR complex on cell surface [8,10]. The result suggests that impairment in the TCR signaling is also present in *Bcl11b*$^{KO/+}$ mice.

TCR or preTCR signaling leads to the activation of a cascade of signaling molecules and eventually to the downstream activation of RAS-MAPK pathway, PI3K-AKT pathway and others [3,27]. Multiple components in the signaling pathway are targeted by either mutations or chromosomal translocations in T-ALL, and the genetic changes result in the activation of TCR or preTCR signaling. Accordingly the activating mutation of TCR or preTCR signaling is classified as a type B abnormality [3]. However, loss of Bcl11b results in an adverse effect, inactivation of the signaling, and hence it may not be a factor contributing to lymphomagenesis.

Difference in cell cycle was observed in radiation-induced injury conditions though not in basal conditions. In both *Bcl11b*$^{+/+}$ and *Bcl11b*$^{KO/+}$ mice, irradiation led to arrest at S and G2/M phase in DP cells but not much in ISP cells. Most ISP cells progressed from S to G1 phase after irradiation, indicating a reduced capability in radiation-induced arrest at ISP stage. Of importance is that the reduced capability of arrest was more marked in *Bcl11b*$^{KO/+}$ mice. This suggests that loss of a *Bcl11b* allele attenuates the cellular response to irradiation that results in arrest at S or G2/M phase. The attenuated cellular response leads to rapid cell cycle progression at S phase, which may decrease the time to repair and hence raise the chance for accumulation of mutations. It was reported that thymocytes at a stage after pre-TCR signaling and before completion of TCRα rearrangement, which includes ISP cells, undergo the malignant transformation in Notch1-activated conditions [28]. Therefore, ISP cells might be cells of origin in thymic lymphomas in *Bcl11b*$^{KO/+}$ mice.

Regulatory role for Bcl11b in cell cycle was studied using Bcl11b knock-down (KD) Jurkat cells, a T-cell culture line [29,30]. Bcl11b-KD cell lines showed cell death with decreased expression of the anti-apoptotic protein Bcl-xL and also a decrease in the CDK inhibitor p27. The decrease of p27 may promote cell cycle progression during S phase. Furthermore, activation of the cell-cycle checkpoint kinase Chk1 was deregulated in Bcl11b-KD cells. The activated Chk1 through phosphorylation leads to arrest of cell cycle at S phase [29]. Therefore, this deregulation may abrogate S phase checkpoint, consistent with the attenuated arrest of ISP cells in irradiated *Bcl11b*$^{KO/+}$ mice.

T-ALL is a heterogeneous disease comprising different genetic abnormalities of oncogenic and tumor suppressive genes that are associated with specific patterns of gene expressions, as determined by microarray analysis [31–33]. Type A abnormalities in T-ALL may delineate distinct molecular-cytogenetic T-ALL subgroups and are thought to cause arrest at a specific stage of normal T-cell differentiation. Results in this study demonstrated that loss of a *Bcl11b* allele in thymocytes affects T-cell differentiation leading to developmental arrest. The arrest may contribute to thymic lymphoma development. However, the consequence was not at a specific stage but at different ISP and DP stages, which may not support that *Bcl11b* mutation belongs to a group of type A abnormalities. Type B abnormalities target cellular processes such as cell cycle regulation. Our results showed that loss of a *Bcl11b* allele impairs cell cycle regulation of ISP cells in radiation-induced injury conditions. This favors that the loss of a *Bcl11b* allele belongs to the group of type B abnormalities, consistent with that *BCL11B* mutations were detected across the major molecular subtypes of T-ALL [22].

Acknowledgments

The authors thank Dr. H. Honda at Hiroshima University for critical reading the manuscript. This work was supported by grants-in-aid of Third Term Comprehensive Control Research for Cancer from the Ministry of Health, Labor and Welfare and for Cancer Research from the Ministry of Education, Science, Technology, Sports, and Culture of Japan. The authors declare no conflict of interest.

Contributions: RG and KT contributed equally to this work and performed the majority of studies; SH performed studies in Fig. 2; YK performed studies in Fig. 3; YA and YM helped design studies in Figs. 3 and 4; RK helped to plan and direct experiments and wrote the manuscript.

Appendix A. Supplementary data

Supplementary data associated with this article can be found, in the online version, at http://dx.doi.org/10.1016/j.leukres.2012.04.028.

References

[1] Armstrong SA, Look AT. Molecular genetics of acute lymphoblastic leukemia. J Clin Oncol 2005;23:6306–15.

[2] Paganin M, Ferrando A. Molecular pathogenesis and targeted therapies for NOTCH1-induced T-cell acute lymphoblastic leukemia. Blood Rev 2011;25:83–90.

[3] Van Vlierberghe P, Pieters R, Beverloo HB, Meijerink JP. Molecular-genetic insights in paediatric T-cell acute lymphoblastic leukaemia. Br J Haematol 2008;143:153–68.

[4] Wakabayashi Y, Inoue J, Takahashi Y, Matsuki A, Kosugi-Okano H, Shinbo T, et al. Homozygous deletions and point mutations of the Rit1/Bcl11b gene in gamma-ray induced mouse thymic lymphomas. Biochem Biophys Res Commun 2003;301:598–603.

[5] Wakabayashi Y, Watanabe H, Inoue J, Takeda N, Sakata J, Mishima Y, et al. Bcl11b is required for differentiation and survival of alphabeta T lymphocytes. Nat Immunol 2003;4:533–9.

[6] Avram D, Fields A, Pretty On Top K, Nevrivy DJ, Ishmael JE, Leid M, et al. Isolation of a novel family of C(2)H(2) zinc finger proteins implicated in transcriptional repression mediated by chicken ovalbumin upstream promoter transcription factor (COUP-TF) orphan nuclear receptors. J Biol Chem 2000;275:10315–22.

[7] Liu P, Li P, Burke S. Critical roles of Bcl11b in T-cell development and maintenance of T-cell identity. Immunol Rev 2010;238:138–49.

[8] Albu DI, Feng D, Bhattacharya D, Jenkins NA, Copeland NG, Liu P, et al. BCL11B is required for positive selection and survival of double-positive thymocytes. J Exp Med 2007;204:3003–15.

[9] Albu DI, VanValkenburgh J, Morin N, Califano D, Jenkins NA, Copeland NG, et al. Transcription factor Bcl11b controls selection of invariant natural killer T-cells by regulating glycolipid presentation in double-positive thymocytes. Proc Natl Acad Sci USA 2011;108:6211–6.

[10] Kastner P, Chan S, Vogel WK, Zhang LJ, Topark-Ngarm A, Golonzhka O, et al. Bcl11b represses a mature T-cell gene expression program in immature CD4(+)CD8(+) thymocytes. Eur J Immunol 2010;40:2143–54.

[11] Li P, Burke S, Wang J, Chen X, Ortiz M, Lee SC, et al. Reprogramming of T cells to natural killer-like cells upon Bcl11b deletion. Science 2010;329:85–9.

[12] Li L, Leid M, Rothenberg EV. An early T cell lineage commitment checkpoint dependent on the transcription factor Bcl11b. Science 2010;329:89–93.

[13] Ikawa T, Hirose S, Masuda K, Kakugawa K, Satoh R, Shibano-Satoh A, et al. An essential developmental checkpoint for production of the T cell lineage. Science 2010;329:93–6.

[14] Shinbo T, Matsuki A, Matsumoto Y, Kosugi S, Takahashi Y, Niwa O, et al. Allelic loss mapping and physical delineation of a region harboring a putative thymic lymphoma suppressor gene on mouse chromosome 12. Oncogene 1999;18:4131–6.

[15] Kominami R, Niwa O. Radiation carcinogenesis in mouse thymic lymphomas. Cancer Sci 2006;97:575–81.

[16] Kamimura K, Ohi H, Kubota T, Okazuka K, Yoshikai Y, Wakabayashi Y, et al. Haploinsufficiency of Bcl11b for suppression of lymphomagenesis and thymocyte development. Biochem Biophys Res Commun 2007;355:538–42.

[17] Ohi H, Mishima Y, Kamimura K, Maruyama M, Sasai K, Kominami R. Multi-step lymphomagenesis deduced from DNA changes in thymic lymphomas and atrophic thymuses at various times after γ-irradiation. Oncogene 2007;26:5280–9.

[18] Przybylski GK, Dik WA, Wanzeck J, Grabarczyk P, Majunke S, Martin-Subero JI, et al. Disruption of the BCL11B gene through inv(14)(q11.2q32.31) results in the expression of BCL11B-TRDC fusion transcripts and is associated with the absence of wild-type BCL11B transcripts in T-ALL. Leukemia 2005;19:201–8.

[19] Keersmaecker K, Real PJ, Gatta GD, Palomero T, Sulis ML, Tosello V, et al. The TLX1 oncogene drives aneuploidy in T cell transformation. Nat Med 2010;16:1321–7.

[20] Gutierrez A, Kentsis A, Sanda T, Holmfeldt L, Chen SC, Zhang J, et al. The BCL11B tumor suppressor is mutated across the major molecular subtypes of T-cell acute lymphoblastic leukemia. Blood 2011;118:4169–73.

[21] Arlotta P, Molyneaux BJ, Chen J, Inoue J, Kominami R, Macklis JD, et al. Neuronal subtype-specific genes that control corticospinal motor neuron development in vivo. Neuron 2005;45:207–21.

[22] Okazuka K, Wakabayashi Y, Kashihara M, Inoue J, Sato T, Yokoyama M, et al. p53 prevents maturation of T cell development to the immature $CD4^{-}CD8^{+}$ stage in $Bcl11b^{-/-}$ mice. Biochem Biophys Res Commun 2005;328:545–9.

[23] Go R, Hirose S, Morita S, Yamamoto T, Katsuragi Y, Mishima Y, et al. Bcl11b heterozygosity promotes clonal expansion and differentiation arrest of thymocytes in gamma-irradiated mice. Cancer Sci 2010;101:1347–53.

[24] Rothenberg EV, Moore JE, Yui MA. Launching the T-cell-lineage developmental programme. Nat Rev Immunol 2008;8:9–21.

[25] Xue L, Nolla H, Suzuki A, Mak TW, Winoto A. Normal development is an integral part of tumorigenesis in T cell-specific PTEN-deficient mice. Proc Natl Acad Sci USA 2008;105:2022–7.

[26] McCormack MP, Young LF, Vasudevan S, de Graaf CA, Codrington R, Rabbitts TH, et al. The Lmo2 oncogene initiates leukemia in mice by inducing thymocyte self-renewal. Science 2010;327:879–83.

[27] Chervinsky DS, Lam DH, Melman MP, Gross KW, Aplan PD. scid Thymocytes with TCRbeta gene rearrangements are targets for the oncogenic effect of SCL and LMO1 transgenes. Cancer Res 2001;61:6382–7.

[28] Li X, Gounari F, Protopopov A, Khazaie K, von Boehmer H. Oncogenesis of T-ALL and malignant consequences of overexpressing intracellular NOTCH1. J Exp Med 2008;205:2851–61.

[29] Kamimura K, Mishima Y, Obata M, Endo T, Aoyagi Y, Kominami R. Lack of Bcl11b tumor suppressor results in vulnerability to DNA replication stress and damages. Oncogene 2007;26:5840–50.

[30] Grabarczyk P, Przybylski GK, Depke M, Völker U, Bahr J, Assmus K, et al. Inhibition of BCL11B expression leads to apoptosis of malignant but not normal mature T cells. Oncogene 2007;26:3797–810.

[31] Ferrando AA, Neuberg DS, Staunton J, Loh ML, Huard C, Raimondi SC, et al. Gene expression signatures define novel oncogenic pathways in T cell acute lymphoblastic leukemia. Cancer Cell 2002;1:75–87.

[32] Soulier J, Clappier E, Cayuela JM, Regnault A, García-Peydró M, Dombret H, et al. HOXA genes are included in genetic and biologic networks defining human acute T-cell leukemia (T-ALL). Blood 2005;106:274–86.

[33] Van Vlierberghe P, van Grotel M, Tchinda J, Lee C, Beverloo HBV, Vander-Spek PJ, et al. The recurrent SET-NUP214 fusion as a new HOXA activation mechanism in pediatric T-cell acute lymphoblastic leukemia. Blood 2008;111:4668–80.

Dig Dis Sci
DOI 10.1007/s10620-012-2239-8

ORIGINAL ARTICLE

Increased Susceptibility to Severe Chronic Liver Damage in CXCR4 Conditional Knock-Out Mice

Atsunori Tsuchiya · Michitaka Imai · Hiroteru Kamimura · Masaaki Takamura · Satoshi Yamagiwa · Tatsuki Sugiyama · Minoru Nomoto · Toshio Heike · Takashi Nagasawa · Tatsutoshi Nakahata · Yutaka Aoyagi

Received: 16 November 2011 / Accepted: 2 May 2012

Abstract
Background The chemokine SDF-1 and its receptor CXCR4 are essential for the proper functioning of multiple organs. In the liver, cholangiocytes and hepatic progenitor cells (HPCs) are the main cells that produce SDF-1, and SDF-1 is thought to be essential for HPC-stimulated liver regeneration.
Aims In this study, CXCR4 conditionally targeted mice were used to analyze the role of SDF-1 in chronically damaged liver.
Methods Chronic liver damage was induced in MxCre CXCR4$^{f/null}$ mice and the control MxCre CXCR4$^{f/wt}$ mice by CCl_4. Serum markers were analyzed to assess liver function and damage, the number of cytokeratin-positive cells as a measure of HPCs, and the extent of liver fibrosis. Additional parameters relating to liver damage, such as markers of HPCs, liver function, MMPs, and TIMPs were measured by real-time PCR.
Results Serum ALT was significantly higher in MxCre CXCR4$^{f/null}$ mice than MxCre CXCR4$^{f/wt}$ mice. The number of cytokeratin-positive cells and the area of fibrosis were also increased in the MxCre CXCR4$^{f/null}$ mice. The expression of mRNAs for several markers related to hepatic damage and regeneration was also increased in the liver of MxCre CXCR4$^{f/null}$ mice, including primitive HPC marker prominin-1, MMP9, TNF-α, and α-SMA.
Conclusions MxCre CXCR4$^{f/null}$ mice were susceptible to severe chronic liver damage, suggesting that SDF-1-CXCR4 signals are important for liver regeneration and preventing the progression of liver disease. Modulation of SDF-1 may therefore be a promising treatment strategy for patients with chronic liver disease.

Keywords SDF-1 · CXCR4 · Chronic liver damage · MMP9 · Liver fibrosis · Hepatic progenitor cells

Abbreviations

SDF-1	Stromal cell-derived factor-1
CXCR4	C-X-C chemokine receptor type 4
HGF	Hepatocyte growth factor
bFGF	Basic fibroblast growth factor
EGF	Epidermal growth factor
OSM	Oncostatin M
HIV	Human immunodeficiency virus
pIpC	Poly(I)-poly(C)
PBS	Phosphate-buffered saline
FACS	Fluorescence-activated cell sorter
FITC	Fluorescein isothiocyanate
PCR	Polymerase chain reaction
ALB	Albumin

A. Tsuchiya (✉) · M. Imai · H. Kamimura · M. Takamura · S. Yamagiwa · M. Nomoto · Y. Aoyagi
Division of Gastroenterology and Hepatology, Graduate School of Medical and Dental Science, Niigata University, 1-757 Asahimachi-dori, Chuo-ku, Niigata 951-8510, Japan
e-mail: atsunori@med.niigata-u.ac.jp

T. Sugiyama · T. Nagasawa
Department of Immunobiology and Hematology, Institute for Frontier Medical Sciences, Kyoto University, 53 Kawahara-cho, Shogoin, Sakyo-ku, Kyoto 606-8507, Japan

T. Heike
Department of Pediatrics, Graduate School of Medicine, Kyoto University, 54 Kawahara-cho, Shogoin, Sakyo-ku, Kyoto 606-8507, Japan

T. Nakahata
Department of Clinical Application, Center for iPS Cell Research and Application, Kyoto University, 54 Kawahara-cho, Shogoin, Sakyo-ku, Kyoto 606-8507, Japan

Published online: 05 June 2012

ALP	Alkaline phosphatase
ALT	Alanine aminotransferase
VEGF	Vascular endothelial growth factor
AFP	α-Fetoprotein
NCAM	Neural cell adhesion molecule
DLK-1	Delta-like 1 homolog
G-6-p	Glucose-6-phosphate
CPS1	Carbamoyl phosphate synthetase 1
cyp	Cytochrome P450
α-SMA	α Smooth muscle actin
TNF-α	Tumor necrosis factor-α
TGF-β	Transforming growth factor-β
MMP	Matrix metalloproteinase
TIMP	Tissue inhibitors of metalloproteinases
GAPDH	Glyceraldehydes-3-phosphate dehydrogenase
TGF	Transforming growth factor

Introduction

The liver has a high regenerative capacity but some severely or chronically damaged livers regenerate poorly despite the presence of numerous hepatic stem/progenitor cells [1, 2]. Liver regeneration from hepatic progenitor cells (HPCs) is stimulated by external factors such as HGF, bFGF, EGF [3, 4], and OSM [5], but also produce their own factors that enhance regeneration, such as stromal cell-derived factor-1 (SDF-1).

SDF-1 is a member of a large family of structurally related chemoattractive cytokines and was first characterized as a growth-stimulating factor for B lymphocyte precursors [6, 7]. The primary physiologic receptor for SDF-1 is CXCR4, a seven-transmembrane receptor coupled to heterotrimeric guanosine triphosphate (GTP)-binding proteins [8, 9]. Mice with a heterozygous SDF-1 or CXCR4 mutation are healthy and fertile. Nagasawa et al. reported that homozygous mutant (SDF-$1^{null/null}$ or $CXCR4^{null/null}$) embryos were present at the expected ratios until day 15.5 of embryogenesis (E15.5); however, about half the SDF-$1^{null/null}$ or $CXCR4^{null/null}$ embryos were dead at E18.5 and all neonates died within an hour of birth [8, 9]. Subsequent studies using targeted gene disruption of SDF-1-CXCR4 signals have indicated that this pathway is essential for B lymphocyte development [8], maintenance of the hematopoietic stem cell pool in the bone marrow stromal cell niche [10, 11], cardiac vascular formation [12, 13], vascularization of the gastrointestinal tract [9, 14], branching morphology in the pancreas [15], and cerebellar formation [16–18].

Within the liver, SDF-1 is mainly produced by cholangiocytes and HPCs and is upregulated in response to injury [19, 20]. Thus, SDF-1 is thought to contribute to HPC-mediated liver regeneration. The reported roles of SDF-1 in liver regeneration are oval cell activation through autocrine/paracrine pathways [19, 20], collagen production through activation and expansion of hepatic stellate cells [21], and angiogenesis through the mobilization of hematopoietic cells [22]. As described above, SDF-1 affects a variety of CXCR4-positive target cells and has multiple functions. Thus, comprehensive analysis of whether SDF-1 act on positively or negatively during the liver damage is very important in assessing its potential for medical treatment to promote liver regeneration.

In this study, we employed MxCre $CXCR4^{f/null}$ mice to comprehensively analyze the role of SDF-1-CXCR4 signals in damaged livers. Using this mouse, we can conditionally delete CXCR4 in damaged livers after the administration of poly(I)-poly(C) (pIpC), using MxCre $CXCR4^{f/wt}$ mice as controls. Using this system, we analyzed the role of the SDF-1-CXCR4 pathway in chronic liver damage resulting from treatment with CCl_4.

Materials and Methods

Mice

To get MxCre-$CXCR4^{f/null}$ mice and MxCre-$CXCR4^{f/wt}$ mice, $CXCR4^{f/null}$ mice were crossed with MxCre mice [23]. MxCre mice and $CXCR4^{f/null}$ mice were kind gifts from Professor Rajewsky (Harvard Medical School) and Professor Lichtenberg (University of Cologne), and Professor Nagasawa (University of Kyoto), respectively. The strain of these mice was C57BL/6. In MxCre mice, Cre is expressed after the induction of interferon by administration of pIpC. CXCR4 floxed mice have a LoxP-CXCR4 conditional targeting allele. Twelve MxCre-$CXCR4^{f/wt}$ mice and ten MxCre-$CXCR4^{f/null}$ mice were employed in this experiment. Eight-week-old mice were injected pIpC (400 μg per mouse, eight times at 2-day intervals; Amersham Biosciences, Piscataway, NJ) intraperitoneally to induce cre expression. After pIpC treatment, 6 weeks was allowed for recovery from the bone marrow suppression induced by pIpC injection. Then, 1 μl/gram per body weight of CCl_4 (Wako, Osaka, Japan) dissolved in olive oil (Wako) (1:4) was injected intraperitoneally twice a week for 8 weeks to induce chronic liver damage. Eight weeks after the first injection of CCl_4, the mice were analyzed (Fig. 1). For analysis, approximately 500 μl of blood was collected from each mouse, liver weight (LW) and body weight (BW) were calculated, and the livers were removed for flow cytometric analysis, immunohistochemistry, or RNA extraction. Deletion of the floxed CXCR4 gene in the liver was detected by flow cytometry and real-time PCR. All animal experiments were conducted in accordance with the guidelines of Niigata University.

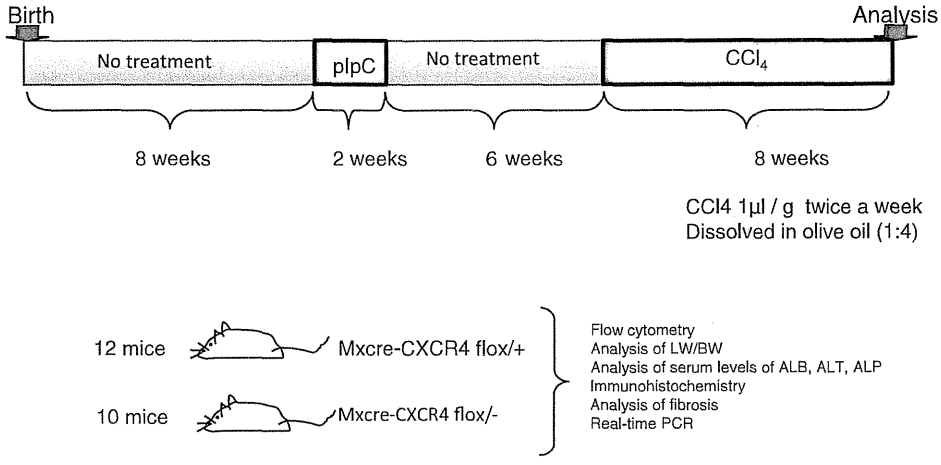

Fig. 1 Summary of experimental approach. MxCre-CXCR4$^{f/null}$ mice and MxCre-CXCR4$^{f/wt}$ mice were employed in this experiment. To delete CXCR4, each mouse was injected with pIpC. After the interval, chronic liver damage was induced by administration of CCl_4. Flow cytometry, analysis of LW/BW, analysis of serum levels of ALB, ALT and ALP, immunohistochemistry, analysis of fibrosis, and real-time PCR were performed to assess the effects of CXCR4 deletion on liver damage

Flow Cytometric Analysis

For flow cytometric analysis, Liver Perfusion Medium (Invitrogen, Carlsbad, CA) and Liver Digest Medium (Invitrogen) were directly injected into the liver. The livers were then minced in 10 ml of Liver Digest Medium and dissociated by gentle MACS® (Miltenyi Biotec, Inc., Auburn, CA). Following dissociation, an equivalent amount of PBS was added and the resulting cell suspension was strained through 70- and 45-μm Cell Strainers (Becton–Dickinson, San Jose, CA), followed by centrifugation at 500 rpm for 1 min to remove centrifuged hepatocytes. The supernatant was centrifuged at 1,000 rpm for 3 min and the centrifuged cells were collected and analyzed using a FACScan (Becton–Dickinson). The antibodies used were FITC conjugated anti-CD45, FITC conjugated anti-CD3, FITC conjugated anti-CD11b, and FITC conjugated anti-CD19 (Becton–Dickinson).

Immunohistochemistry

SDF-1 immunohistochemistry was performed on CCl_4-damaged liver from MxCre-CXCR4$^{f/wt}$ mice and chronic-damaged human liver. For cytokeratin immunohistochemistry, CCl_4 damaged livers of MxCre-CXCR4$^{f/null}$ mice and MxCre-CXCR4$^{f/wt}$ mice were employed. Liver tissue was fixed in 10 % formalin and embedded in paraffin blocks. Four-micrometer sections were cut and mounted on silane-coated slides. For immunohistochemical analysis, paraffin was removed and antigen retrieval was performed using antigen retrieval solution for anti-SDF-1 (BioGenex Laboratories, San Ramon, CA) for 15 min in a microwave oven or using proteinase K for anti-cytokeratin. Endogenous peroxidase activity was blocked with 3 % hydrogen peroxide in methanol (Wako) for 10 min at room temperature, and sections were incubated overnight with the primary antibody, mouse anti-SDF-1 antibody (R&D Systems, Inc., Minneapolis, MN), or anti-cytokeratin antibody that can detect bile duct and hepatic progenitor cells (Dako, Glostroup, Denmark) diluted in PBS. Slides were then stained using the Vectastain® ABC kit (Vector Laboratories, Inc., Burlingame, CA) and DAB TRIS tablets (Muto Pure Chemicals, Tokyo, Japan). Anti-cytokeratin-positive cells that located deep in the lobule and did not form part of ducts were counted. We counted 20 randomly selected fields/screen at 100× magnification.

Real-Time PCR

Total RNA was isolated from the livers using the RNeasy Mini kit (Qiagen, Chatsworth, CA) according to the manufacturer's protocol; 1 μg of total RNA was used as a template for the synthesis of cDNA using the Transcriptor First Strand cDNA Synthesis kit (Roche Applied Science, Mannheim, Germany). Aliquots of cDNA were subjected to real-time PCR using a LightCycler System (Roche Applied Science). The TaqMan probe and primer sets were purchased from Applied Biosystems (Foster City, CA) (Table 1). PCR conditions were as follows: 95 °C for 10 min followed by 45 cycles of 95 °C for 10 s, 60 °C for 30 s, and 72 °C for 1 s. The results were normalized to the level of mRNA for human glyceraldehyde-3-phosphate dehydrogenase (GAPDH).

Analysis of Fibrosis

Formalin-fixed liver sections were stained with Picrosirius Red Stain Kit (Polysciences, Inc. Warrington, PA). Sirius

Table 1 Name of TaqMan probe and primer sets and their assay identification number

Name	Identification number
CXCR4	Mm01292123_m1
SDF-1	Mm00445553_m1
Prominin-1	Mm01211408_m1
AFP	Mm00431715_m1
NCAM	Mm01149710_m1
DLK-1	Mm00494477_m1
α-SMA	Mm01546133_m1
TNF-α	Mm99999068_m1
TGF-β	Mm01178820_m1
TIMP1	Mm00441818_m1
TIMP3	Mm00441827_m1
MMP2	Mm00439491_m1
MMP9	Mm00442991_m1
MMP13	Mm00439491_m1
MMP14	Mm01318966_m1

Red staining was quantitated by ImageJ software in three randomly selected fields/section at 100× magnification.

Statistics

Statistical analyses were performed using GraphPad Prism 5 software (GraphPad Software, Inc., La Jolla, CA). The results were assessed using the Mann–Whitney test. Differences were considered significant when the p value was less than 0.05.

Results

Induced Deletion of CXCR4 in Adult Mouse Livers

The presence of SDF-1-producing cells in mouse and human liver was confirmed by immunohistochemistry. As previously reported, SDF-1-producing cells were located in the bile ducts and cells of ductular reaction that were thought to include HPCs (Fig. 2a, b) [19, 20]. The staining pattern was common between human and mice. Deletion of CXCR4 was confirmed by flow cytometry using liver hematopoietic cells and real-time PCR using liver tissues. In five of the ten MxCre-CXCR4$^{f/null}$ mice, the frequency of CD19+ B lymphocytes in CD45+ hematopoietic cells was significantly reduced (Fig. 2c) and the frequency of CD11b+ monocyte in CD45+ cells was significantly increased (Fig. 2d) in comparison to MxCre-CXCR4$^{f/wt}$ mice. The frequency of CD3+ T cells in CD45+ hematopoietic cells was also increased but this was not statistically significant (Fig. 2e). SDF-1 was first characterized as a pre-B-lymphocyte growth stimulation factor and is essential for B lymphocyte development [6, 7]. Thus, our results suggest that in five of ten MxCre-CXCR4$^{f/null}$ mice, CXCR4 was efficiently deleted. CXCR4 mRNA expression in the liver of these five CXCR4-deleted mice was significantly lower than in MxCre-CXCR4$^{f/wt}$ mice (Fig. 2f). Thus, these five MxCre-CXCR4$^{f/null}$ mice were used for further analysis. No significant differences in SDF-1 mRNA expression were detected between MxCre-CXCR4$^{f/wt}$ and MxCre-CXCR4$^{f/null}$ mice (Fig. 2g).

The Serum Levels of ALT in MxCre-CXCR4$^{f/null}$ Mice Were Significantly Higher Than in MxCre-CXCR4$^{f/wt}$ Mice

To analyze liver damage by CCl_4 in MxCre-CXCR4$^{f/wt}$ mice and MxCre-CXCR4$^{f/null}$ mice, we measured LW/BW, serum levels of ALB, ALT, and ALP. There were no significant differences in LW/BW between the two groups (Fig. 2g). There were no significant difference in the serum levels of ALB and ALP (Fig. 2h, i), but serum ALT was significantly higher in MxCre-CXCR4$^{f/null}$ mice (3,306 ± 5,327 IU/l) than in MxCre-CXCR4$^{f/wt}$ mice (463 ± 323 IU/l) (Fig. 2j), which suggests that there is severe liver damage in the MxCre-CXCR4$^{f/null}$ mice.

The Number of Hepatic Stem/Progenitor Cells was Increased in MxCre-CXCR4$^{f/null}$ Mice

HPCs were enumerated using an anti-cytokeratin antibody, which stains bile duct and HPCs. The number of anti-cytokeratin-positive cells in MxCre-CXCR4$^{f/null}$ mice (159.1 ± 48.7 cells/field) was significantly higher than in MxCre-CXCR4$^{f/wt}$ mice (81.8 ± 32.2 cells/field) (Fig. 3a–c). To detect altered expression of HPC markers in conditional CXCR4-deleted mice, mRNA levels of prominin-1, AFP, NCAM, and DLK-1 were measured. The mRNA levels of AFP and particularly of prominin-1 were increased in the liver of MxCre-CXCR4$^{f/null}$ mice, while the levels of NCAM and DLK-1 were not affected by CXCR4 targeting (Fig. 3d–g). Prominin-1 is a primitive hepatic stem/progenitor marker [2, 24], and these results therefore suggest that activation of hepatic stem/progenitor cells occurred more strongly in MxCre-CXCR4$^{f/null}$ mice than in MxCre-CXCR4$^{f/wt}$ mice.

Increased Liver Fibrosis in MxCre-CXCR4$^{f/null}$ Mice

Liver fibrosis in tissue sections was analyzed by Sirius Red staining, which identifies areas of collagen accumulation. The extent of Sirius Red staining was significantly higher in the liver of MxCre-CXCR4$^{f/null}$ mice (2.7 ± 0.6 %) than in MxCre-CXCR4$^{f/wt}$ mice (1.6 ± 0.5 %) (Fig. 4a–c). To confirm our results, mRNA expression of a range of markers of liver fibrosis were measured; mRNA of stellate cell

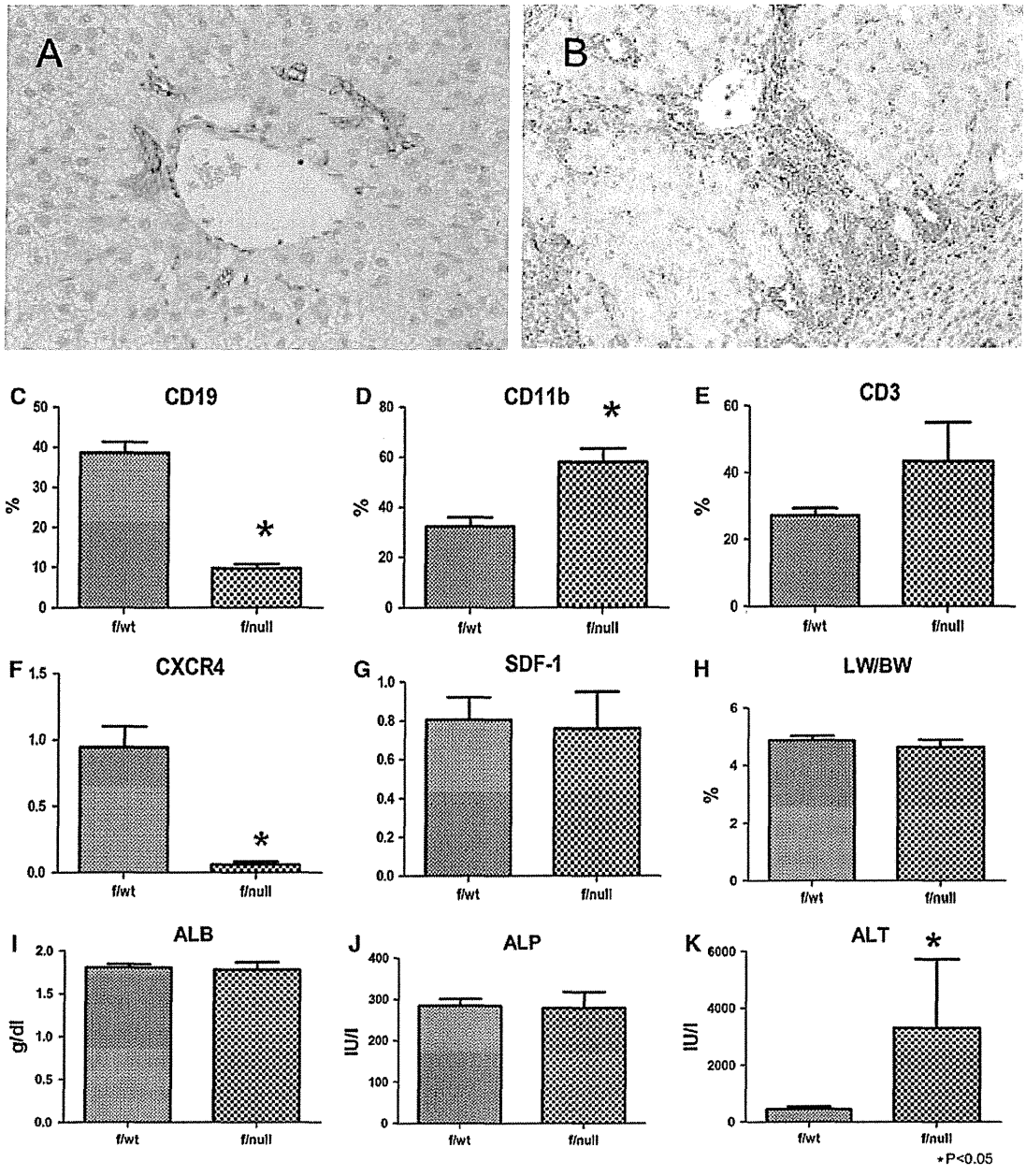

Fig. 2 Immunohistochemistry for SDF-1 (**a**, **b**), flow cytometric analysis of hematopoietic cells in the liver (**c**–**e**), and analysis of CXCR4 and SDF-1 mRNA in the liver (**g**, **f**). In both the mouse (**a**) and human (**b**) livers, cholangiocytes and HPCs express SDF-1. Flow cytometric analysis of CD19 (**c**), CD11b (**d**), and CD3 cells (**e**) in CD45 cells revealed that CD19 cells were significantly decreased and CD11b and CD3 cells were increased in five of ten MxCre-CXCR4$^{f/null}$ mice. Real-time PCR analysis revealed that in these five mice, although the mRNA of SDF-1 was not different (**g**), the mRNA levels of CXCR4 were significantly decreased (**f**). Analysis of LW/BW (**h**) and serum levels of liver markers (**i**–**k**). LW/BW was not different between the two groups (**h**). The serum levels of ALB (**i**), ALP (**j**) were not different, but the serum levels of ALT (**k**) in MxCre-CXCR4$^{f/null}$ mice were significantly higher than in MxCre-CXCR4$^{f/wt}$ mice

markers (α-SMA, TNF-α, and TGF-β), the mRNA levels of MMPs (MMP2, MMP9, MMP13, and MMP14) and the mRNA levels of TIMPs (TIMP1 and TIMP3). The expression of α-SMA and TNF-α mRNA was significant higher in MxCre-CXCR4$^{f/null}$ mice than in MxCre-CXCR4$^{f/wt}$ mice (Fig. 4d, e), while the expression of TGF-β mRNA was not changed (Fig. 4f). These results suggest enhanced activation of some signals of stellate cells in the liver of MxCre-CXCR4$^{f/null}$ mice. In the mRNA levels of the MMPs, the mRNA of MMP9 was significantly increased in the liver of MxCre-CXCR4$^{f/null}$ mice (Fig. 4g–j). There were no differences in expression of the TIMP mRNAs between the two

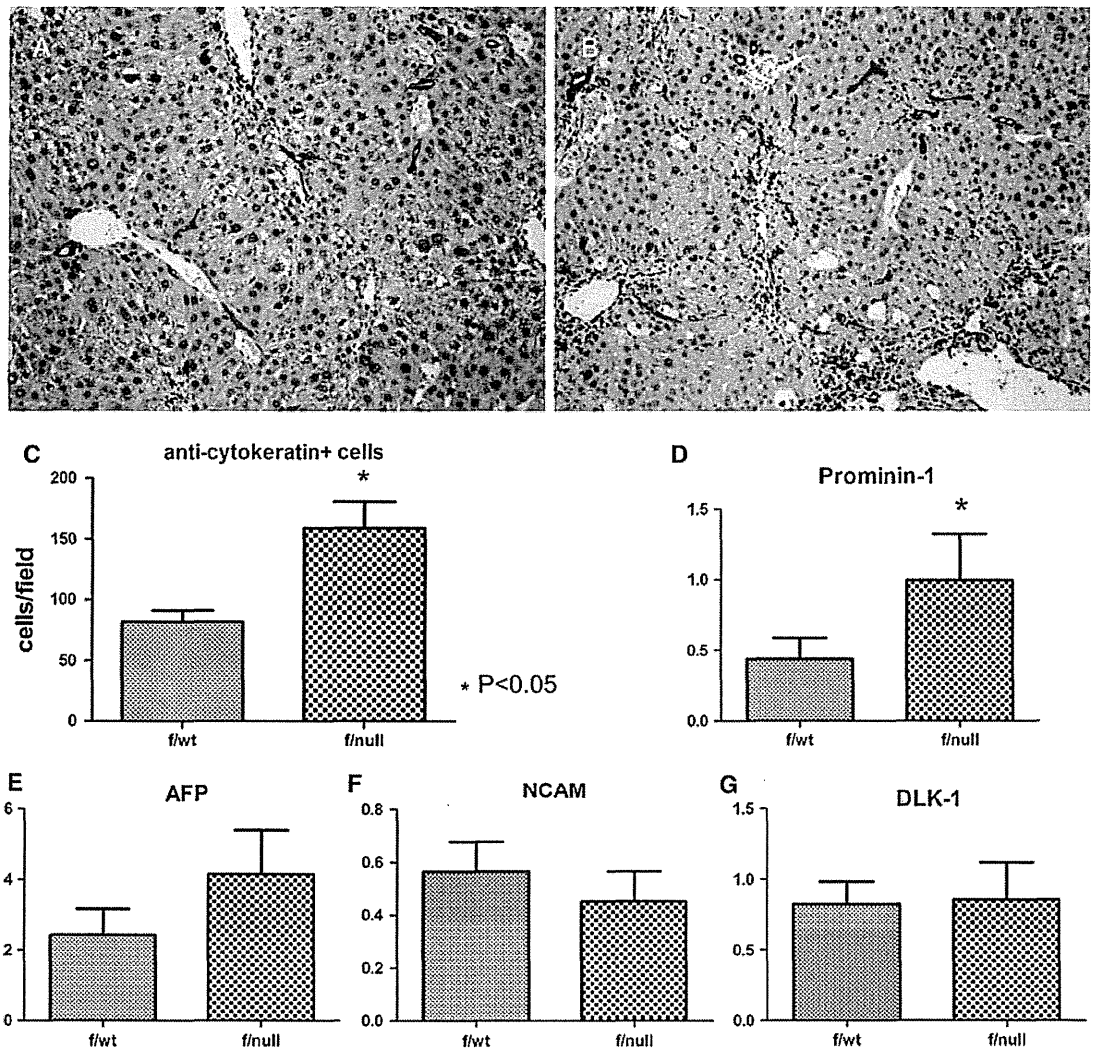

Fig. 3 Immunohistochemistry for detection of cytokeratin-positive cells (**a–c**) and real-time PCR analysis of HPC markers (**d–g**). Analysis of MxCre-CXCR4$^{f/wt}$ mice (**a**) and MxCre-CXCR4$^{f/null}$ mice (**b**) revealed that the number of cytokeratin-positive cells in the liver of MxCre-CXCR4$^{f/null}$ mice was significantly higher than in MxCre-CXCR4$^{f/wt}$ mice (**c**). Analysis of HPC markers revealed that mRNA expression of the most primitive HPC marker prominin-1 was significantly higher in MxCre-CXCR4$^{f/null}$ mice (**d**). AFP mRNA expression was higher in MxCre-CXCR4$^{f/null}$ mice, but the difference was not significant (**e**). The mRNA levels of NCAM (**f**) and DLK-1 (**g**) were not affected by CXCR4 targeting

groups (Fig. 4k, l). The activation of some signals of stellate cells and up-regulation of the MMP9 mRNA in MxCre-CXCR4$^{f/null}$ mice are consistent with the results suggesting severe liver damage in the MxCre-CXCR4$^{f/null}$ mice.

Discussion

Previous reports have shown that SDF-1-CXCR4 signals are essential for the function of multiple organs such as bone marrow [6–8, 10, 11], brain [16–18], heart [12, 13], and blood vessels [9, 14]. However, the contribution of SDF-1-CXCR4 signals to the pathogenesis of chronic liver damage is not known. In this study, we analyzed the role of SDF1-CXCR4 signals in CCl_4-induced chronic liver damage in CXCR4 conditionally targeted mice. MxCre-CXCR4$^{f/null}$ mice suffered enhanced liver damage compared with MxCre-CXCR4$^{f/wt}$ mice. Furthermore, the number of HPCs was increased in the liver of MxCre-CXCR4$^{f/null}$ mice, but the HPCs did not appear to undergo full differentiation and liver fibrosis was severe. We conclude that SDF-1-CXCR4 signaling contributes to hepatic protection and liver regeneration.

Several previous studies have analyzed SDF-1-CXCR4 signals in the liver; however, their conclusions varied somewhat from our study. Mavier et al. reported that SDF-1 stimulates the proliferation of HPCs through an autocrine/paracrine pathway [19] and Zheng et al. reported

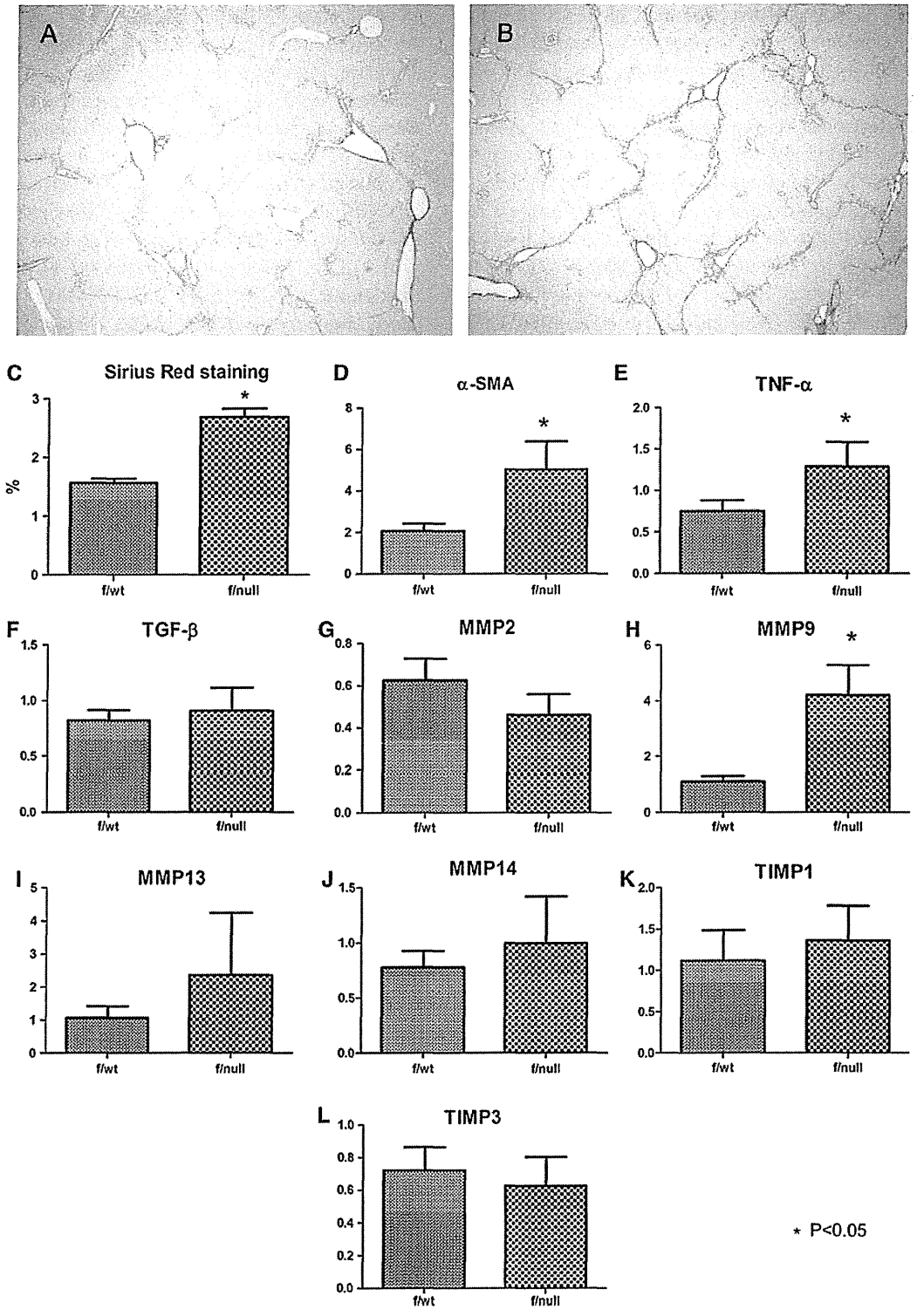

Fig. 4 Analysis of fibrosis by Sirius Red staining (**a–c**) and real-time PCR analysis of hepatic stellate cells markers, TIMPs, and MMPs (**d–l**). Sirius Red staining of MxCre-CXCR4$^{f/wt}$ (**a**) and MxCre-CXCR4$^{f/null}$ mice (**b**) revealed that the extent of the area of fibrosis (*red area*) in MxCre-CXCR4$^{f/null}$ mice was significantly higher than in MxCre-CXCR4$^{f/wt}$ mice (**c**). The mRNA levels of α-SMA and TNF-α were significant higher in the livers of MxCre-CXCR4$^{f/null}$ mice than in MxCre-CXCR4$^{f/wt}$ mice (**d**, **e**) but the mRNA levels of TGF-β were not different (**f**). The mRNA levels of MMP2 (**g**), MMP13 (**i**), MMP14 (**j**), TIMP1 (**k**) and TIMP3 (**l**) were not different, but the mRNA level of MMP9 (**h**) was significantly higher in the MxCre-CXCR4$^{f/null}$ mice than in the MxCre-CXCR4$^{f/wt}$ mice

that SDF-1 is essential for activation of HPCs [20]. Our analysis revealed that the number of cytokeratin-positive cells, which includes hepatic stem/progenitor cells, was increased in the liver of CXCR4 conditionally deleted mice. Furthermore, expression of prominin-1 mRNA, which is a marker for the most primitive hepatic stem/progenitor cells, was increased significantly in the liver of CXCR4 conditional deleted mice. Our results suggest that SDF-1-CXCR4 signals promote liver regeneration. The difference between our study and the studies of Zheng et al. and Mavier et al. may be due to differences in the animal models or drugs used. We consider that mice with CXCR4 targeted specifically in hepatic stem/progenitor cells will be very valuable in resolving these issues.

Hong et al. reported that SDF-1-CXCR4 signals are important for HSC activation, fibrogenesis, and proliferation [21]. These authors also suggested that small molecular inhibitors of CXCR4 may have antifibrotic properties. However, in our study, liver fibrosis was exacerbated in CXCR4 conditionally deleted mice, which was further confirmed by the up-regulation of mRNAs for MMP9, TNF-α, and α-SMA. Thus, our results indicate that SDF-1-CXCR4 signals are important for preventing the progression of liver fibrosis, and that blocking this pathway may not be a safe strategy for the treatment of liver damage.

Glunwald et al. reported that SDF-1 is important for retention of a pro-angiogenic subpopulation of hematopoietic cells in the liver [22]. One caveat to our study is the differing hematopoietic cell populations in the MxCre-CXCR4$^{f/null}$ and MxCre-CXCR4$^{f/wt}$ mice; the MxCre-CXCR4$^{f/null}$ mice have a reduction in B lymphocyte number and a slight increase in monocytes in the liver. We cannot exclude the possibility that the differences in the hematopoietic cells populations influenced the results. However, CXCR4 is expressed by multiple cell types, and it is not currently possible to specifically target CXCR4 on specific cells. Nonetheless, our study clearly suggests that SDF-1-CXCR4 signals are important in liver regeneration and hepatic protection.

In our study, CXCR4 was effectively deleted in MxCre-CXCR4$^{f/null}$ mice, however the mRNA of SDF-1 was not different between the two groups. Kojima et al. reported that SDF-1 affect the production of SDF-1 by feed-forward manner [25]. Thus we think that although MxCre-CXCR4$^{f/null}$ mice had more anti-cytokeratin-positive cells, the production of SDF-1 per cell was lower in MxCre-CXCR4$^{f/null}$ mice.

It may be possible to exploit our findings to develop new treatments to promote liver regeneration. SDF-1-CXCR4 signals can be modulated by external factors. Leucocyte-derived protease or cell-surface-expressed CD26/dipeptidylpeptidase IV (DPPIV) can cleave both SDF-1 and the N-terminus of CXCR4 [26], and DPPIV activity is known to be increased in chronically damaged livers [27]. Therefore, protease inhibitors may have value for preventing the cleavage of SDF-1 and CXCR4 in the liver. DPPIV inhibitors have already been widely used to treat type 2 diabetes mellitus, and they may also promote liver regeneration and hepatic protection by preventing the cleavage of SDF-1 and CXCR4. Furthermore, SDF-1-CXCR4 signals can be modulated by a broad range of mediators, both positively (e.g., PMV, C3a, des-arg C3a, thrombin, uPAR, fibronectin, hyaluronic acid, sICAM1, and cVCAM1) and negatively (e.g., lipopolysaccharide (LPS), heparin, MIP-1α, and PATENT) [26]. Therefore, modulation of SDF-1 production by HPCs is an additional strategy for stimulation of liver regeneration and hepatic protection.

Acknowledgments We thank Professor Rajewsky (Harvard Medical School) and Professor Lichtenberg (University of Cologne) for providing MxCre mice. This research was supported by Tsukada memorial grant, by a Grant-in Aid for Young Scientists (B, 22790634) of The Ministry of Education, Culture, Sports, Science and Technology and by a Grant for Promotion of Niigata University Research Project.

Conflict of interest None.

References

1. Forbes S, Vig P, Poulsom R, et al. Hepatic stem cells. *J Pathol.* 2002;197:510–518.
2. Tsuchiya A, Kamimura H, Takamura M, et al. Clinicopathological analysis of CD133 and NCAM human hepatic stem/progenitor cells in damaged livers and hepatocellular carcinomas. *Hepatol Res.* 2009;39:1080–1090.
3. Tsuchiya A, Heike T, Fujino H, et al. Long-term extensive expansion of mouse hepatic stem/progenitor cells in a novel serum-free culture system. *Gastroenterology.* 2005;128:2089–2104.
4. Tsuchiya A, Heike T, Baba S, et al. Long-term culture of postnatal mouse hepatic stem/progenitor cells and their relative developmental hierarchy. *Stem Cells.* 2007;25:895–902.
5. Miyajima A, Kinoshita T, Tanaka M, et al. Role of oncostatin M in hematopoiesis and liver development. *Cytokine Growth Factor Rev.* 2000;11:177–183.
6. Nagasawa T, Kaisho T, Kishimoto T, et al. Generation and characterization of a monoclonal antibody that inhibits stromal cell-dependent B lymphopoiesis. *J Immunol.* 1994;152:2788–2797.
7. Nagasawa T, Kikutani H, Kishimoto T. Molecular cloning and structure of a pre-B-cell growth-stimulating factor. *Proc Natl Acad Sci USA.* 1994;91:2305–2309.
8. Nagasawa T, Hirota S, Tachibana K, et al. Defects of B-cell lymphopoiesis and bone-marrow myelopoiesis in mice lacking the CXC chemokine PBSF/SDF-1. *Nature.* 1996;382:635–638.
9. Tachibana K, Hirota S, Iizasa H, et al. The chemokine receptor CXCR4 is essential for vascularization of the gastrointestinal tract. *Nature.* 1998;393:591–594.
10. Tokoyoda K, Egawa T, Sugiyama T, et al. Cellular niches controlling B lymphocyte behavior within bone marrow during development. *Immunity.* 2004;20:707–718.
11. Sugiyama T, Kohara H, Noda M, et al. Maintenance of the hematopoietic stem cell pool by CXCL12-CXCR4 chemokine

signaling in bone marrow stromal cell niches. *Immunity*. 2006;25: 977–988.
12. Cheng Z, Liu X, Ou L, et al. Mobilization of mesenchymal stem cells by granulocyte colony-stimulating factor in rats with acute myocardial infarction. *Cardiovasc Drugs Ther*. 2008;22: 363–371.
13. Sanematsu F, Hirashima M, Laurin M, et al. DOCK180 is a Rac activator that regulates cardiovascular development by acting downstream of CXCR4. *Circ Res*. 2010;107:1102–1105.
14. Ara T, Tokoyoda K, Okamoto R, et al. The role of CXCL12 in the organ-specific process of artery formation. *Blood*. 2005;105: 3155–3161.
15. Hick AC, van Eyll JM, Cordi S, et al. Mechanism of primitive duct formation in the pancreas and submandibular glands: a role for SDF-1. *BMC Dev Biol*. 2009;9:66.
16. Stumm RK, Zhou C, Ara T, et al. CXCR4 regulates interneuron migration in the developing neocortex. *J Neurosci*. 2003;23: 5123–5130.
17. Zhu Y, Yu T, Zhang XC, et al. Role of the chemokine SDF-1 as the meningeal attractant for embryonic cerebellar neurons. *Nat Neurosci*. 2002;5:719–720.
18. Zhu Y, Matsumoto T, Mikami S, et al. SDF1/CXCR4 signalling regulates two distinct processes of precerebellar neuronal migration and its depletion leads to abnormal pontine nuclei formation. *Development*. 2009;136:1919–1928.
19. Mavier P, Martin N, Couchie D, et al. Expression of stromal cell-derived factor-1 and of its receptor CXCR4 in liver regeneration from oval cells in rat. *Am J Pathol*. 2004;165:1969–1977.
20. Zheng D, Oh SH, Jung Y, et al. Oval cell response in 2-acetylaminofluorene/partial hepatectomy rat is attenuated by short interfering RNA targeted to stromal cell-derived factor-1. *Am J Pathol*. 2006;169:2066–2074.
21. Hong F, Tuyama A, Lee TF, et al. Hepatic stellate cells express functional CXCR4: role in stromal cell-derived factor-1alpha-mediated stellate cell activation. *Hepatology*. 2009;49:2055–2067.
22. Grunewald M, Avraham I, Dor Y, et al. VEGF-induced adult neovascularization: recruitment, retention, and role of accessory cells. *Cell*. 2006;124:175–189.
23. Kuhn R, Schwenk F, Aguet M, et al. Inducible gene targeting in mice. *Science*. 1995;269:1427–1429.
24. Rountree CB, Barsky L, Ge S, et al. A CD133-expressing murine liver oval cell population with bilineage potential. *Stem Cells*. 2007;25:2419–2429.
25. Kojima Y, Acar A, Eaton EN, et al. Autocrine TGF-β and stromal cell-derived factor-1 (SDF-1) signaling drives the evolution of tumor-promoting mammary stromal myofibroblast. *Proc Natl Acad Sci USA*. 2010;107:20009–20014.
26. Kucia M, Jankowski K, Reca R, et al. CXCR4-SDF-1 signalling, locomotion, chemotaxis and adhesion. *J Mol Histol*. 2004;35: 233–245.
27. Balaban YH, Korkusuz P, Simsek H, et al. Dipeptidyl peptidase IV (DDP IV) in NASH patients. *Ann Hepatol*. 2007;6:242–250.

Hepatology Research

Hepatology Research 2013; 43: 139–146 doi: 10.1111/j.1872-034X.2012.01088.x

Review Article

Role of gut microbiota in liver diseases

Yasuhiro Miyake and Kazuhide Yamamoto

Department of Gastroenterology and Hepatology, Okayama University Graduate School of Medicine, Dentistry and Pharmaceutical Sciences, Okayama, Japan

The liver constantly encounters food-derived antigens and bacterial components such as lipopolysaccharide translocated from the gut into the portal vein. Bacterial components stimulate Toll-like receptors (TLR), which are expressed on Kupffer cells, biliary epithelial cells, hepatocytes, hepatic stellate cells, endothelial cells and dendritic cells and recognize specific pathogen-associated molecular patterns. The signaling of TLR to its main ligand triggers inflammation. Usually, in order to protect against hyperactivation of the immune system and to prevent organ failure by persistent inflammation, TLR tolerance to repeated stimuli is induced. In chronic liver diseases, a breakdown in TLR tolerance occurs. Furthermore, Kupffer cells, hepatic stellate cells and natural killer T cells are key components of innate immunity. Decreased numbers and impaired ability of these cells lead to failures in immune tolerance, resulting in persistent inflammation. Recently, the activation of inflammasome was revealed to control the secretion of pro-inflammatory cytokines such as interleukin-1β in response to bacterial pathogens. Innate immunity seems to be an important contributor to the pathogenesis of fatty liver disease and autoimmune liver disease. Recently, probiotics were reported to affect various liver diseases via shifts in gut microbiota and the stability of intestinal permeability. However, many unresolved questions remain. Further analysis will be needed to gain a more comprehensive understanding of the association of innate immunity with the pathogenesis of various liver diseases.

Key words: gut microbiota, inflammasome, innate immunity, probiotic, tolerance, Toll-like receptor

INTRODUCTION

THE LIVER, THE largest organ in the body, weight 1200–1500 g and has a double blood supply.[1] The hepatic artery, coming from the celiac axis, supplies the liver with arterial blood and the portal vein brings venous blood from the intestines and spleen. Portal blood flow in humans is approximately 1000–1200 mL/min. Thus, the liver constantly confronts food-derived antigens and bacterial components such as lipopolysaccharide (LPS) translocated from the gut into the portal vein; however, the liver has the unique capacity to induce immune tolerance.

Previously, regulatory T cells (Treg), Kupffer cells, natural killer T (NKT) cells and hepatic stellate cells (HSC) were reported to contribute to immune tolerance in the liver. Interaction between Treg and Kupffer cells promotes the secretion of interleukin (IL)-10 from Treg, and the depletion of Treg breaks antigen-specific immune tolerance.[2] The depletion of liver NKT cells also exacerbates hepatic inflammation in carbon tetrachloride-induced liver injury.[3] HSC induce the apoptosis of conventional $CD4^+$ T cells in a Fas/Fas ligand-dependent manner and increase Treg proliferation via cell–cell contact; moreover, HSC-expanded Treg express high levels of programmed cell death 1 and cytotoxic T-lymphocyte antigen 4, show enhanced production of IL-10, and cause the suppression of alloreactive $CD4^+$ T-cell proliferation.[4]

Toll-like receptors (TLR), which comprise a highly conserved family of receptors that recognizes specific pathogen-associated molecular patterns (PAMP), play a key role in innate immunity by triggering inflammatory responses to the main ligands of TLR. Various TLR are expressed on liver cells (Table 1). The liver constantly encounters various antigens, and in order to prevent organ failure due to hyperactivation of the immune system, TLR tolerance to repeated stimuli is induced.[11] On the other hand, a breakdown in TLR tolerance

Correspondence: Dr Yasuhiro Miyake, Department of Gastroenterology and Hepatology, Okayama University Graduate School of Medicine, Dentistry, and Pharmaceutical Sciences, 2-5-1 Shikata-cho, Kita-ku, Okayama 700-8558 Japan. Email: miyakeyasuhiro@hotmail.com
Received 31 May 2012; revision 24 July 2012; accepted 15 August 2012.